Fall 12-2014

The *Drosophila* T-box Transcription Factor Midline Functions within the Insulin/AKT and c-Jun-N-terminal Kinase Signaling Pathways to Regulate Interomatidial Bristle Formation and Cell Survival

Qichuan Chen
University of Southern Mississippi

The University of Southern Mississippi

THE *DROSOPHILA* T-BOX TRANSCRIPTION FACTOR MIDLINE FUNCTIONS WITHIN THE INSULIN/AKT AND C-JUN-N-TERMINAL KINASE SIGNALING PATHWAYS TO REGULATE INTEROMMATIDIAL BRISTLE FORMATION AND CELL SURVIVAL

by

Qichuan Chen

A Thesis
Submitted to the Graduate School
of The University of Southern Mississippi
in Partial Fulfillment of the Requirements
for the Degree of Master of Science

Approved:

Dr. Sandra Leal
Committee Chair

Dr. Hao Xu

Dr. Janis O'Donnell

Dr. Karen Coats
Dean of the Graduate School

December 2014

ABSTRACT

THE *DROSOPHILA* T-BOX TRANSCRIPTION FACTOR MIDLINE FUNCTIONS WITHIN THE INSULIN/AKT AND C-JUN-N-TERMINAL KINASE SIGNALING PATHWAYS TO REGULATE INTEROMMATIDIAL BRISTLE FORMATION AND CELL SURVIVAL

by Qichuan Chen

December 2014

From a genetic and allelic modifier screen, we report that the *Drosophila melanogaster* T-box transcription factor *midline (mid),* a homolog to the human *TBX20* gene, interacts with *dFOXO* within the insulin receptor (InR) and the c-Jun-N-terminal kinase (JNK) signaling pathways to regulate interommatidial bristle (IOB) formation. Previous studies have identified *mid*'s role in cell fate specification of sensory organ precursor cells in conjunction with the Notch-Delta signaling pathway (Das et al., 2013). The Notch, InR, and JNK signaling pathways regulate dFOXO activity under conditions of stress. Thus, we determined the effects of oxidative stress and metabolic stress by exposing *mid*-RNAi flies to paraquat and starvation conditions, respectively. We found that oxidative stress suppressed the *mid*-RNAi phenotype while starvation had no significant effect. We next assayed Mid and H15, a paralog of Mid, via Western blot analysis and report that Mid exhibits a nucleocytoplasmic distribution pattern that is altered within the *mid*-RNAi mutant while H15 was found exclusively within the cytoplasmic fraction. This opens the possibility that Mid and/or H15 may regulate cytoplasmic targets upstream of dFOXO. The evidence suggests that Mid utilizes the InR,

JNK, and Notch signaling pathways to regulate cell fate specification, differentiation, and survival during third instar larval development.

DEDICATION

I would like to dedicate this thesis to my family, whose unconditional support has motivated me through the completion of this thesis as well as in all of my endeavors.

ACKNOWLEDGMENTS

It takes a village to raise a child. I could not have completed this thesis without the support of my thesis advisor, my committee members, my family, and my friends.

I would first like to express my deepest gratitude to my thesis advisor Dr. Sandra Leal. Her unwavering support has laid the foundation for my scientific success. Her door was always open whenever I found myself in a quandary about my thesis. I am very grateful for her guidance, financial support, and passion for science. I will forever owe her ice cream.

Additionally, I would like to thank my committee members, Dr. Hao Xu and Dr. Janis O'Donnell, for taking the time to help me achieve my academic goals. Their participation and feedback was critical in shaping and focusing my thesis.

A special thanks goes to the members of my lab. Sudeshna Das provided a lot of guidance and training to get me ready for science without my training wheels. She was the calm before the storm that was Petra Visac and Kendrick D. Buford. I would like to thank these two for providing a jovial atmosphere during the most critical points of completing this thesis.

Finally, I must thank the rag-tag crew that helped me count more than half a million eye bristles as well as provided conversation in the lab: Wisam Buti, Slater Smith, Kelly Odom, Brielle Menegazzi, Ian Thorton, Natasha Major, Marli Bryant, Hannah Lee, and Lily Brady.

TABLE OF CONTENTS

LIST OF TABLES

Table

LIST OF ILLUSTRATIONS

Figure

CHAPTER I

INTRODUCTION

The *midline* Gene Expresses a T-box Transcription Factor

The *Drosophila melanogaster* T-box transcription factor *midline (mid)* gene, a homolog of human *TBX20*, has been shown to regulate the cell fate specification and organogenesis of the developing heart, CNS, and eye tissues (Das et al., 2013; Leal, Qian, Lacin, Bodmer, & Skeath, 2009; Miskolczi-McCallum, Scavetta, Svendsen, Soanes, & Brook, 2005; Qian, Liu, & Bodmer, 2005; Reim, Mohler, & Frasch, 2005). Members of the large T-box transcription factor protein family, characterized by a conserved, palindromic T-box DNA-binding domain, are expressed in a vast array of vertebrate and invertebrate organisms (Degnan et al., 2009; Muller & Herrmann, 1997). In mammalian species, this transcription factor family consists of 18 genes within 5 subfamilies: Tbx1 (*TBX1, TBX10, TBX15, TBX18, TBX20,* and *TBX22*), Tbx2 (*TBX2, TBX3, TBX4*, and *TBX5*), Tbx6 (*TBX6* and *TBX16*), T (*T-BRAIN1, EOMESODERMIN, T-BET,* and *TBX21*), and Brachyury (*BRACHYURY* and *TBX19*). Within *Drosophila*, the family contains eight genes: *brachyenteron, dorsocross-1, dorsocross-2, dorsocross-3, optomotor-blind, optomotor-blind-related-gene-1, H15, and mid* (Buescher et al., 2004; Griffin et al., 2000; Penton, Selleck, & Hoffman, 1997; Poeck, Hofbauer, & Pflugelder, 1993; Porsch et al., 1998; Reim et al., 2003).

Development of the *Drosophilia* Eye

Located within the compound eye of *Drosophila melanogaster* are the ommatidia, which form a highly organized neurocrystalline lattice structure containing a field of approximately 800 ommatidial units (Waddington & Perry, 1960; Perry, 1968; Ready et

al., 1976). Found within each ommatidial unit are eight photoreceptor neurons referred to as R1-R8 cells that are located below four lens-secreting cone cells and surrounded by two primary pigment cells (Tomlinson & Ready, 1987) (Figure 1). Enclosing the R1-R8 photoreceptor cluster are six secondary pigment cells, three tertiary pigment cells, and three bristle cells that are shared with adjacent photoreceptor clusters (Ready, Hanson, & Benzer, 1976). This arrangement of ommatidial units across the eye results in a total of approximately 400 interommatidial bristle (IOB) complexes that each contain a shaft cell, socket cell, sheath cell, and sensory neuron.

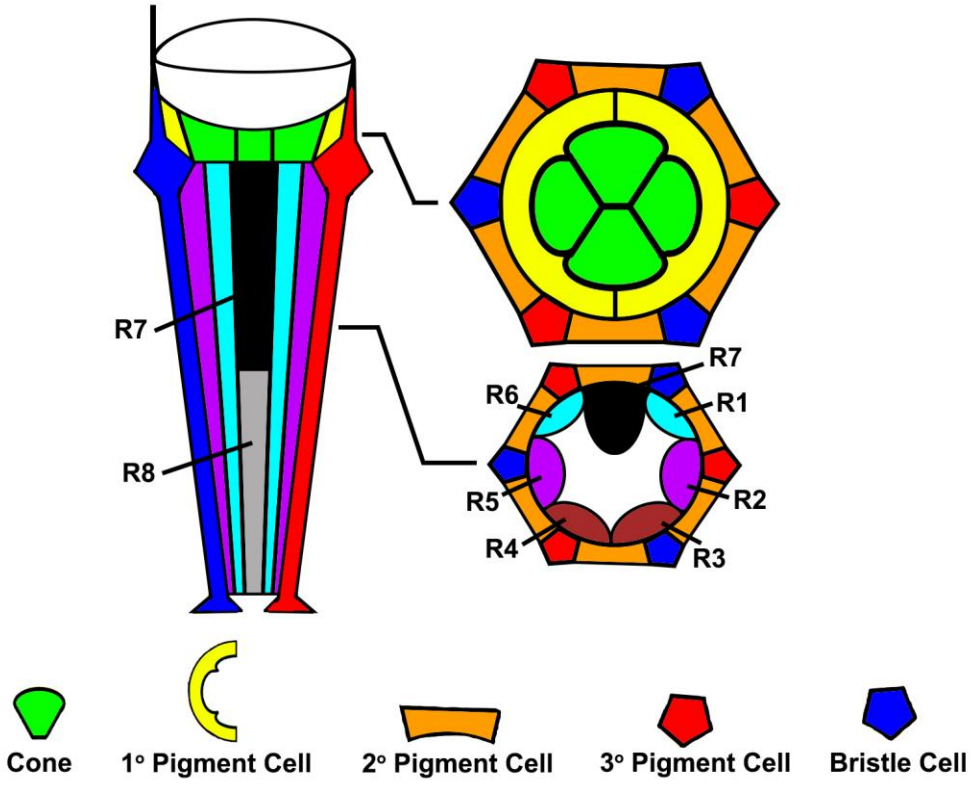

Figure 1. A schematic diagram of the ommatidial unit. The superficial ommatidial unit consists of 4 cone cells (green) underneath a lens (white dome) and surrounded by 2 primary pigment cells (yellow). These cells share 3 bristles (blue), 6 secondary (orange) and 3 tertiary (red) pigment cells with adjacent ommatidial units. Deeper within the ommatidial unit, the R1-R6 photoreceptor cells surround the R7 (black) and R8 (gray) cells. The R7 cell is located superficial to the R8 cell.

The development of the *Drosophilia* eye begins within the eye-antennal imaginal disc during the third-instar larval stage in which a wave of differentiating epithelial cells called the morphogenetic furrow moves across the eye imaginal disc from the posterior region to the anterior region (Figure 2). This wave of differentiation compresses the monolayer of epithelial cells that comprise the imaginal disc and is then delimited by the morphogenetic gradient created by several retinal determination transcription factors including Hedgehog (Hh), Decapentaplegic (Dpp), and Wingless (Wg) (Greenwood & Struhl, 1999; Heberlein, Wolff, & Rubin, 1993; Treisman & Rubin, 1995; Wiersdorff, Lecuit, Cohen, & Mlodzik, 1996). Within the morphogenetic furrow, Hh initiates a signaling cascade to create a Dpp gradient that activates *ato*, a proneural gene which generates intermediate groups. Once this morphogenetic furrow continues anteriorly, the selected posterior proneural cells begin to specify the R8 cells and subsequently recruit the remaining photoreceptor cells to form a photoreceptor neuron cluster (Curtis & Mlodzik, 2000). Anterior to the morphogenetic furrow, however, the cells largely remain undifferentiated as a result of Wg inhibition of Hh and Dpp (Treisman & Rubin, 1995). Recently, studies have hypothesized that the Dpp morphogenetic gradient created in the morphogenetic furrow crosses into the pre-proneural zone anterior to the morphogenetic furrow and selects grandmother pre-SOP (GPS) cells (Das et al., 2013). The GPS cells are postulated to be held in stasis until the pupal stage of development (Das et al., 2013).

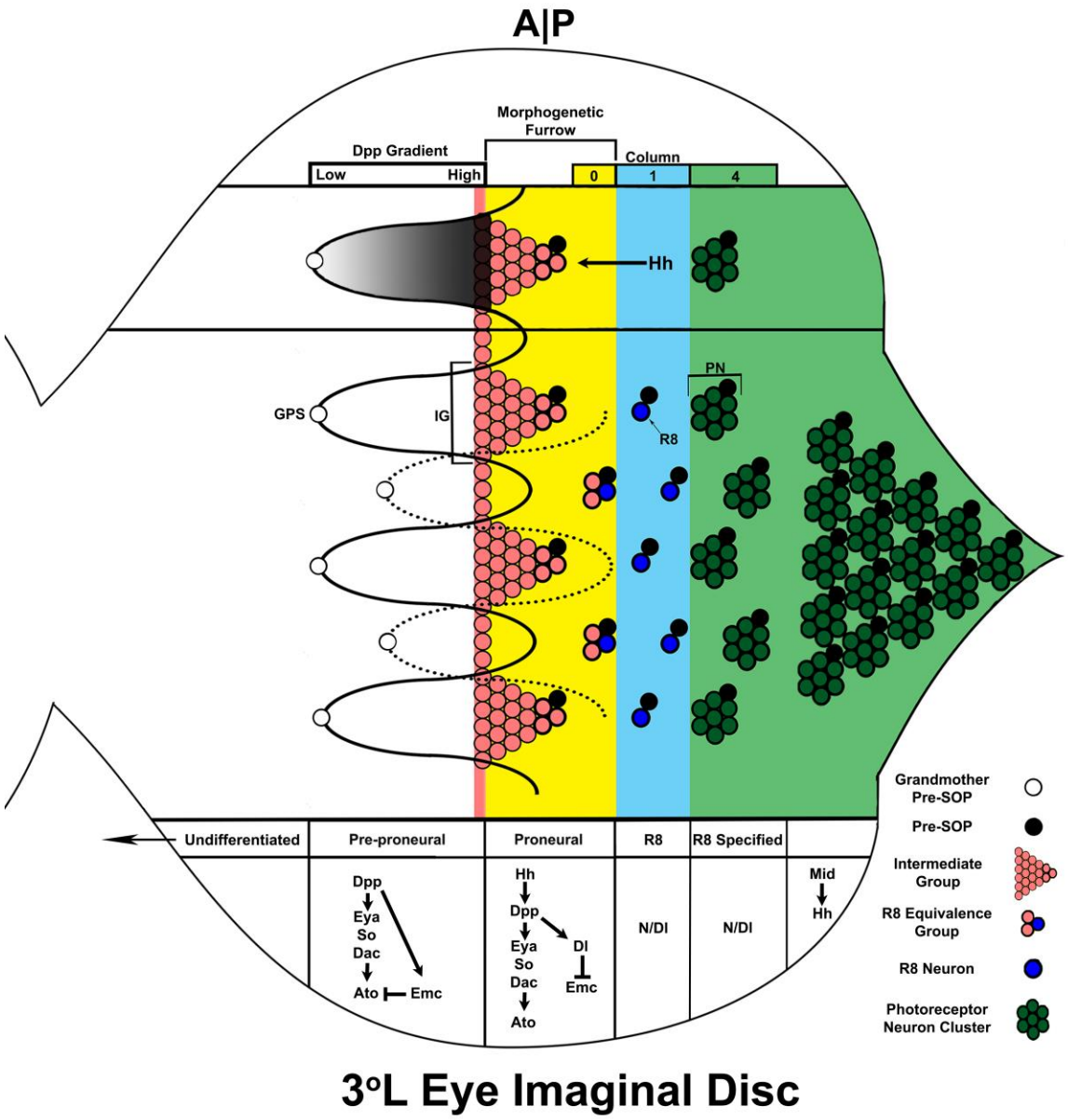

Figure 2. Model of sensory organ precursor selection within the eye imaginal disc. The morphogenetic furrow (yellow column) establishes a *dpp* gradient (scalloped lines) from high (black) to low (light gray) anterior to the furrow. In this pre-proneural zone anterior to the morphogenetic furrow, the low *dpp* signaling begins selection of the grandmother pre-SOP (white circle). As the morphogenetic furrow moves anteriorly, *hh* secreted from posterior SOP cells blocks *dpp* signal and initiates R8 neuron (blue circle) selection from the intermediate group via Notch/Delta lateral inhibition. From there, the R8 neuron recruits R1-7 photoreceptor neurons to form a photoreceptor neuron cluster (green rosetta). *mid* potentially activates *hh* signaling in the posterior photoreceptor neuron clusters.

The Notch/Delta signal transduction pathway functions to select a single neuronal SOP cell surrounded by epithelial cells that have assumed "default" fates via a lateral inhibition mechanism. This neuronal cell fate adoption requires increased expression of proneural proteins Achaetae (Ac) and Scute (Sc) in addition to increased expression of a Notch receptor transmembrane ligand, Delta (Artavanis-Tsakonas, Matsuno & Fortini, 1995; Cubas, de Celis, Campuzano, & Modolell, 1991; Muskavitch, 1994; Skeath & Carroll, 1991; Skeath & Carroll, 1994; Skeath & Doe, 1996) (Figure 3).

Once selected, proneural SOP cells express Delta ligands and activate the Notch receptors of neighboring cells via juxtacrine signaling (Schroeter, Kisslinger, & Kopan, 1998) (Figure 3B). The activation of Notch causes a cleavage of the Notch receptor allowing the Notch intracellular domain (N_{ICD}) to translocate into the nucleus, complex with Mastermind (Mam), and remove the co-repressors of Su(H): Groucho (Gro), Hairless (H), and the C-terminal Binding Protein (CtBP) (Barolo & Posakony, 2002; Barolo, Stone, Bang, & Posakony, 2002; Helms et al., 1999; Nagel et al., 2005; Nagel & Preiss, 2011; Nam, Piotr, Pear, Aster, & Blacklow, 2007). The removal of Su(H)'s co-repressors switches Su(H) from a co-inhibitor of the gene *Enhancer of Split* [*E(spl)*] into a co-activator (Ligoxygakis, Yu, Delidakis, & Baker, 1998). Upon activation, *E(spl)* guides the cells into an epithelial cell fate by inhibiting the expression of *ac* and *sc* (Jimenez & Ish-Horowicz, 1997). Within the Delta-sending, proneural SOP cells, however, *ac* and *sc* expression is increased as a result of the undisturbed co-repression complex on Su(H) (Castro, Barolo, Bailey, & Posakony, 2005).

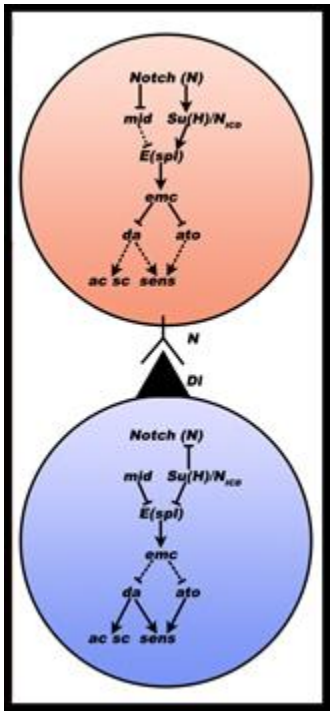

Figure 3. A schematic diagram of Notch signaling pathway. The Notch receptor is activated upon Delta binding and the Notch intracellular domain (N_{ICD}) is cleaved. The N_{ICD} translocates into the nucleus to regulate the expression of the *E(spl)* gene complex.

Concurrent to the lateral inhibition of neighboring cells, the SOP cell undergoes Notch regulated asymmetric division to produce the cellular components of the mechanosensory bristle complex (Hartenstein & Campos-Ortega, 1984). The SOP cell (pI neuroblast) first divides into two precursor cells, pIIa and pIIb, and asymmetrically segregates Numb, a Notch antagonist, toward the pIIb cell (Figure 4) (Rhyu, Jan, & Jan, 1994). The pIIb cell then utilizes the Notch signaling pathway to prevent pIIa from adopting the same cell fate and blocks Notch signaling from pIIa with Numb (Rhyu et al., 1994). This process is repeated with the division of pIIa into a socket and shaft cell where the shaft cell receives the asymmetric load of Numb (Rhyu et al., 1994). Similarly, the pIIb cell divides into a pIIIb cell and a glial cell (Rhyu et al., 1994). The glial cell eventually migrates away from the bristle complex while the pIIIb cell again

utilizes the asymmetric segregation of Numb and Notch signaling to produce a sheath cell and neuron (Rhyu et al., 1994).

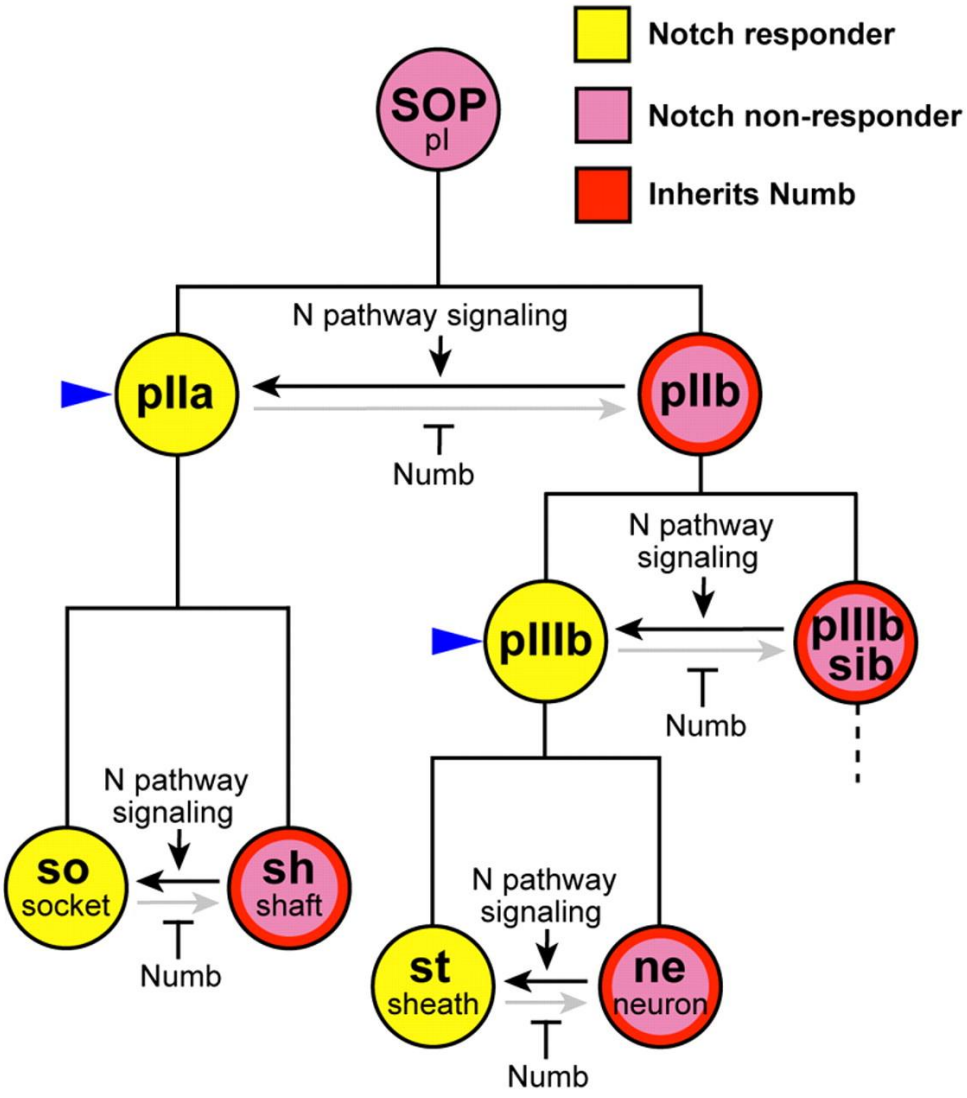

Figure 4. The Numb/Notch interaction dictates asymmetric cell division of SOP cells. pI neuroblasts divide into pIIa and pIIb precursor cells and segregate Numb asymmetrically. Numb in the pIIb cell blocks Notch signaling to pIIb while pIIb initiates Notch signaling within pIIa. pIIa divides into two cells of which the Numb inheriting cell adopts the shaft cell fate and the Notch responder adopts the socket cell fate. pIIb divides with the inheritor of Numb adopting the neuroglia cell fate and the Notch responder, pIIIb, dividing further. The Notch responder of the pIIIb division adopts the sheath cell fate while the non-responder adopts the neuron cell fate. (Rebeiz, Miller & Posakony, 2011, pp. 215-225).

mid and *TBX20* Regulation of Eye Development

While *mid* and *TBX20* have been extensively studied within the developing heart and CNS (Leal et al., 2009; Miskolczi-McCallum et al., 2005; Qian et al., 2005; Reim et al., 2005), recent research has only begun to unravel *mid*'s function within the developing *Drosophila* eye (Das et al., 2013). In mice, *Tbx20* is highly expressed within the neural retina periphery and within the optic cup of early-staged fetuses (Meins, Henderson, Bhattacharya, & Sowden, 2000). In adult mice, *Tbx20* is expressed in the neural retina, pigment epithelium, and optic nerve (Meins et al., 2000). *TBX20* expression is detected in the neural retina, pigment epithelium, optic nerve, and sclera in human fetal eye tissue (Kraus, Haenig, & Kispert, 2001; Meins et al., 2000). By week 13 of gestation in humans, *TBX20* expression in the ganglion cell layer and neuroblastic layer of the neural retina is higher than in the sclera, optic nerve, and cornea (Meins et al., 2000). In *Drosophila* third-instar larvae (3^{o}L), *mid* is highly expressed in the photoreceptor neurons of the imaginal eye-antennal disc (Das et al., 2013). The *mid* gene has been found to regulate the cell fate specification of proneural SOP cells into neuronal ganglion mother cells via the Notch/Delta signaling pathway (Das et al., 2013) (Figure 3).

mid is an Anti-apoptotic Factor

Recently, Das et al. (2013) reported an increase of caspase-3 signaling in the eye-antennal imaginal discs of *mid*-RNAi strains suggesting that *mid* functions as an anti-apoptotic factor during early eye development. Moreover, studies of the vertebrate *mid* homolog *TBX20* have shown that *TBX20* regulates estrogen-mediated cardiomyocyte protection by suppressing apoptosis within mouse and human hearts under oxidative stress conditions (Shen et al., 2013). The anti-apoptotic response triggers the down-

regulation of p38 mitogen-activated protein kinase (MAPK), caspase-3, and Bax while activating Bcl-2, an inhibitor of apoptosis (Shen et al., 2013). The p38 MAPK is a member of the mitogen-activated protein kinase family responsive to stress conditions. Caspase-3 is a member of the caspase signaling cascade that initiates programmed cell death (Han, Richter, Li, Kravchenko, & Ulevitch, 1995). Lastly, Bax and Bcl-2 function antagonistically within the intrinsic apoptotic pathway. Bax disrupts the lipid bilayer of the outer mitochondrial membrane causing destabilization (Renault, Teijido, Antonsson, Dejean, & Manon, 2013). Conversely, Bcl-2 prevents destabilization of the outer membrane (Renault et al., 2013). Permeabilization of the mitochondrial membrane by Bax2 creates pores that allow for the release of cytochrome *c* from the mitochondria. Release of cytochrome *c* into the cytoplasm activates the caspase cascade which results in apoptosis. Taken together, these studies suggest that *mid* and *Tbx20* are functionally conserved.

The regulation of apoptosis within the T-Box transcription factor family is not limited to the Mid and Tbx20 T-box transcription factors. *Brachyury* mutants in *Xenopus laevis* and mouse tissues exhibit high levels of apoptosis (Conlon & Smith, 1999). Conversely, in mouse embryonic fibroblast, the expression of *TBX3* promotes cell survival through the inhibition of the tumor suppressor protein *p53* (Carlson, Ota, Song, Chen, & Hurlin, 2002). Most members of the T-box transcription factor family, however, have not been shown to regulate cell survival.

mid Interacts with *dFOXO*

In an effort to further understand *mid* function within the developing eye, the Leal lab carried out a genetic modifier screen to identify *mid*-interacting genes. From this

screen, the lab identified *dFOXO* as a *mid*-interacting gene (Das et al., 2012). The *dFOXO* gene encodes a Forkhead Box Subgroup O transcription factor vital for the regulation of apoptosis, cell cycle arrest, and DNA repair. The dFOXO transcription factor is also responsive to metabolic, oxidative, and genotoxic stress responses (Brunet et al., 1999; Calnan & Brunet, 2008; Kannan & Fridell, 2013; Wang, Bohmann, & Jasper, 2005). dFOXO plays a significant and evolutionarily conserved role downstream of both the Insulin/Insulin-like receptor (InR) signal transduction pathway and c-Jun N-terminal Kinase (JNK) signal transduction pathway (Essers et al., 2004; Garofalo, 2002; Ikeya, Galic, Belawat, Nairz, & Hafen, 2002; Luo, Puig, Hyun, Bohmann, & Jasper, 2007; Wang et al., 2005) (Figure 5). The JNK signaling pathway is a mitogen-activated protein kinase (MAPK) family member conferring cellular resistance to stress. The discovery of a functional collaboration between *mid* and *dFOXO* promises to yield further insight into *mid*'s role as an anti-apoptotic factor.

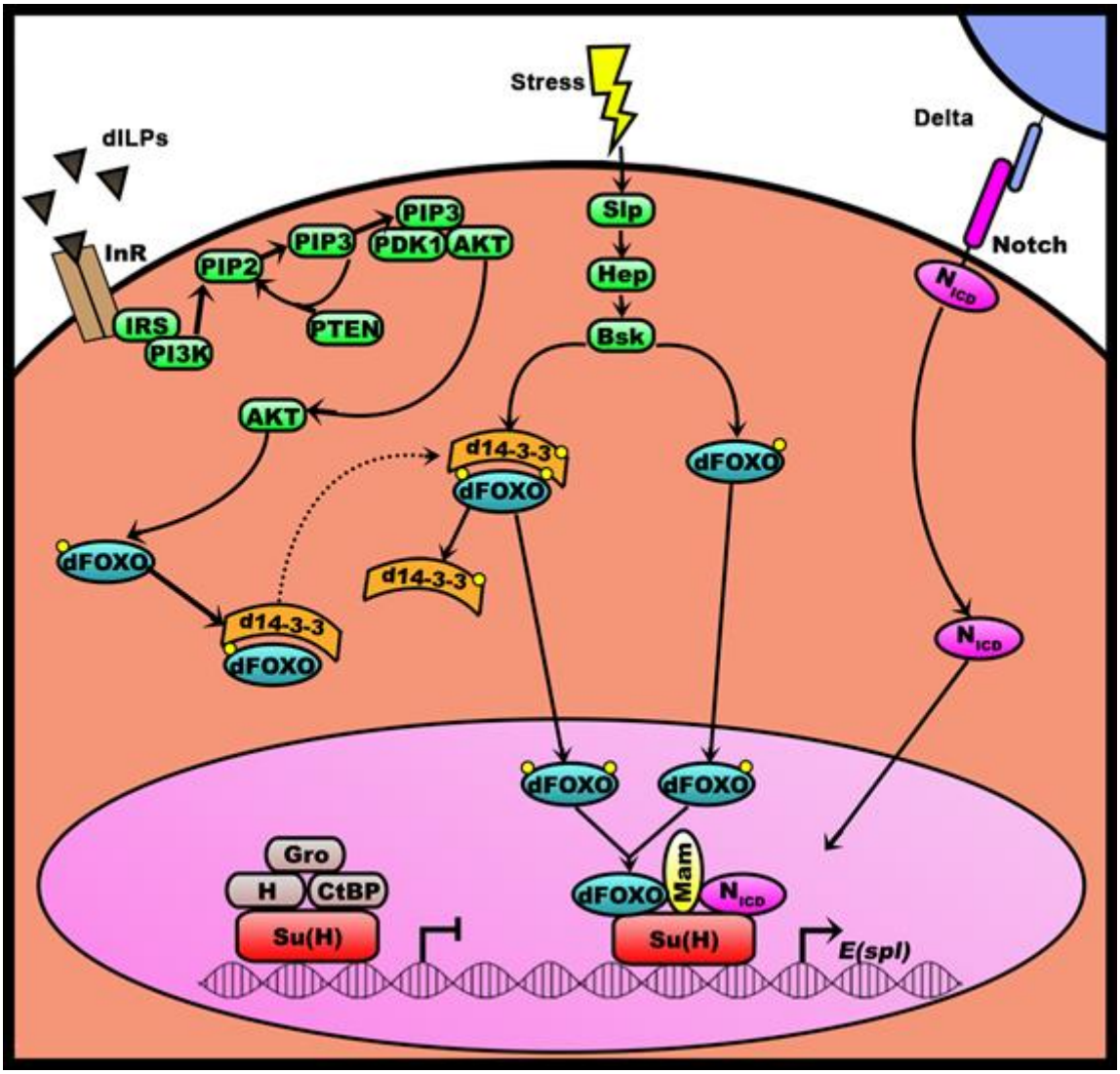

Figure 5. Schematic depiction of the InR and JNK signaling pathway to regulate the Notch signaling pathway. The InR/PI3K/Akt and JNK signal transduction pathways regulate transcription by affecting the specific phosphorylation status of dFOXO where the d14-3-3 protein is required for dFOXO to shuttle into the nucleus. Alternatively, the dFOXO protein can shuttle into the nucleus independently of d14-3-3 downstream of the JNK pathway via phosphorylation of an alternative site by Bsk (JNK).

The InR and JNK are Stress Signaling Pathways

The InR pathway regulates cell survival and apoptosis mediated by the action of secreted insulin and insulin-like peptides (dILPs) released from neurosecretory cells in the brain known as insulin-like peptide producing cells (IPCs) (Puig, Marr, Ruhf, & Tijan, 2003; Puig & Tijan, 2005; Tettweiler, Miron, Jenkins, Sonenberg, & Lasko, 2005).

A humoral link between the fat body and larval brain stimulates dILPs release from IPCs (Geminard, Rulifson, & Leopold, 2009). In *Drosophila*, dILP2, dILP5, and dILP6 circulating within the hemolymph bind to dimeric InR, a receptor tyrosine kinase complex, and stimulate the autophosphorylation of an intracellular carboxyl-terminal domain leading to a cascade of phosphorylation events driven by adaptor proteins and several kinases (Figure 5) (Grewal, 2009; Hay, 2011; Nielsen, Luo, Biteau, Syverson, & Jasper, 2008; Rulifson, Kim, & Nusse, 2002). Activated InR recruits the adaptor protein Chico, a homolog of the insulin receptor substrate (IRS), which interacts and activates phosphatidyl inositol 3'-OH kinase (PI3K), a protein located within the plasma membrane, via an SH2 domain (Clancy et al., 2001; Leevers, Weinkove, MaDougall, Hafen, & Waterfield, 1996). Activated PI3K phosphorylates phosphotidyl inositol 4,5 bisphosphate (PIP_2) and converts the protein into phosphotidyl inositol 3,4,5-triphosphate (PIP_3). Conversely, the tumor suppressor phosphatase and tensin homolog (PTEN) reverts PIP_3 back into PIP_2 (Maehama et al., 2004; Oldham et al., 2002). PIP_3 recruits dAKT (also known as protein kinase B or PKB) by binding to the pleckstrin homology domain within dAKT and exposes the T308 site for recruitment and phosphorylation by phosphoinositide dependent kinase 1 (PDK1) (Georgescu, 2011). Phosphorylation of dAKT at S473 by target of rapamyacin (TOR) or DNA-dependent protein kinases (DNA-PK) leads to a fully activated dAKT that regulates substrate-specific downstream targets in both the cytoplasm and the nucleus (Lu, Huang, & Basu, 2006; Zhang, Stallock, Ng, Reinhard, & Neufeld, 2000). Pleckstrin homology domain leucine-rich repeat protein phosphatase (PHLPP) directly dephosphorylates dAKT at S473 while protein phosphatase 2A (PP2A) dephosphorylates dAKT at T308 (Garofalo et al., 2003; Kuo et

al., 2007). Additionally, polyphosphorylation of dAKT at both T308 and S473 sites triggers partial ubiquitination by the E3 ubiquiting-protein ligase Neural Precursor Cell Expressed Developmentally Down-regulated 4 (NEDD4) (Vecchione, Marchese, Henry, Rotin, & Morrione, 2003).

Conversely, the c-Jun N-terminal kinase (JNK) pathway in *Drosophila* is a signaling cascade that includes the JNKKK *slipper* (*slp*), JNKK *hemipterous* (*hep*) and JNK *basket* (*bsk*) (Glise, Bourdon, & Noselli, 1995; Hay, 2011; Riesgo-Escovar, Jenni, Fritz, & Hafen, 1996; Sluss et al., 1996; Weston & Davis, 2007) (Figure 5). Transcription of the vertebrate targets of JNK is regulated by the TF activator-protein 1 (AP-1), a complex of Jun and Fos, and is conserved in *Drosophilia* with Bsk phosphorylation of D-Jun and D-Fos. This AP1 complex of heterodimerized D-Jun:D-Fos promotes expression of *puckered* (*puc*), a MAPK phosphatase that feedback inhibits *bsk* (Glise & Noselli, 1997; Kockel, Homsy, & Bohmann, 2001). Connector-of-kinase to AP-1 (Cka), a scaffold protein, assists in the JNK pathway in both the cytosol as well as in the nucleus. In the cytoplasm, Cka recruits phosphorylated Hep and unphosphorylated Bsk which results in the phosphorylation of Bsk (Chen et al., 2002). Within the nucleus, Cka assists Bsk to phosphorylate AP-1 (Chen et al., 2002).

Stress Signaling Pathways Regulate dFOXO

dFOXO is a downstream target of the InR and JNK stress-signaling pathways that function antagonistically. Active dAkt phosphorylates dFOXO, thereby allowing d14-3-3 to bind to dFOXO (Nielsen et al., 2008). The evolutionarily conserved 14-3-3:dFOXO complex blocks dFOXO's nuclear localization signal and ultimately sequesters dFOXO within the cytoplasm (Figure 6) (Brunet et al., 1999; Puig et al., 2003; Tzivion, Dobson,

& Ramakrishnan, 2011; Vanhaesebroeck & Aless, 2000; Vanhaesebroeck & Waterfield, 1999). Under conditions of metabolic stress, however, cytoplasmic dFOXO is hypophosphorylated and translocates back into the nucleus. In the nucleus, dFOXO regulates the expression of several target genes including *myc*, *4e-bp*, *glucose-6-phosphatase* (*G6P*), and *InR* (Junger et al., 2003; Luo et al., 2007; Mattila, Kallojarvi, & Puig, 2008; Puig et al., 2003; Puig & Tijan, 2005). *dFOXO* also acts as a positive transcriptional feedback regulator by activating the expression of the *InR* (Puig et al., 2003).

Under conditions of adequate nutrition, dAkt phosphorylates dFOXO to create a docking site for which d14-3-3 can bind and sequester dFOXO in the cytoplasm. Under conditions of oxidative stress, however, the JNK signaling pathway antagonizes the InR signaling pathway by promoting the nuclear translocation of cytosolic-sequestered dFOXO bound to the d14-3-3 protein (Hay, 2011). In human cell culture, activated JNK induces phosphorylation of both FOXO3 and 14-3-3, resulting in the release of FOXO3 from the complex and promotion of FOXO3 nuclear translocation (Figure 6). (Sunayama, Tsuruta, Mayuyama, & Gotoh, 2005; Tsuruta et al., 2004). Previous chromatin immunoprecipitation followed by sequencing (ChIP-seq) and RNA-seq data examining differential expression of genes also report that within the adult mouse heart, genes involved in stress, immune response, and development were downregulated in TBX20 ablated mice compared to wild type mice (Sakabe et al., 2012). Conversely, genes essential for metabolism were found to be upregulated (Sakabe et al., 2012).

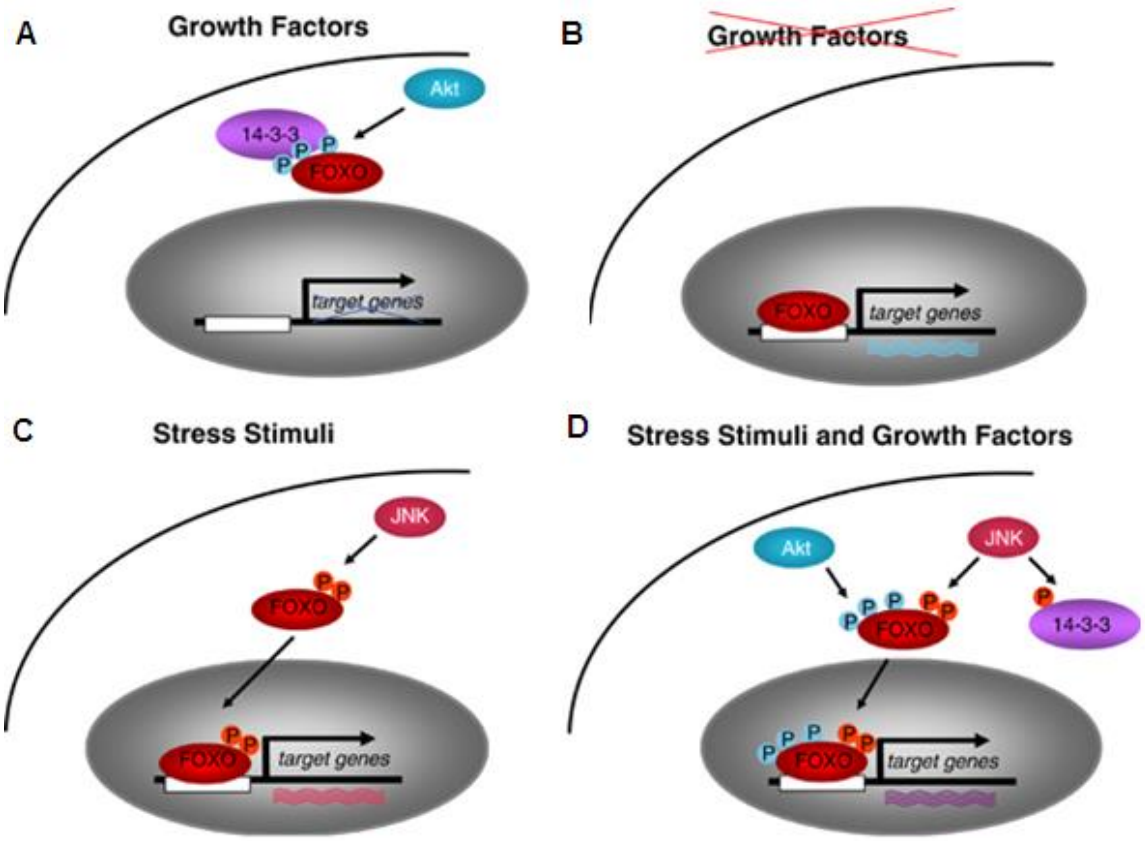

Figure 6. InR and JNK signaling pathways are balanced to regulate dFOXO. A) Under normal conditions, dAkt blocks dFOXO nuclear localization by phosphorylating dFOXO to create a d14-3-3 docking site. B) Under conditions of nutritional stress, dAkt is inactive allowing dFOXO to translocate into the nucleus. C) Under conditions of oxidative or genotoxic stress, the JNK pathway is activated to phosphorylate dFOXO at a separate site. This phosphorylation results in dFOXO translocation into the nucleus. D) Under conditions of adequate nutrition and oxidative stress, dAkt is activated creating the d14-3-3 docking site. Active JNK phosphorylates dFOXO at a separate location and also phosphorylates d14-3-3. Phosphorylation of d14-3-3 releases dFOXO from the d14-3-3 and allows dFOXO to enter into the nucleus. (Greer & Brunet, 2005, pp. 7410-7425).

Thesis Objectives

This thesis seeks to establish whether the T-box transcription factor gene, *midline*, interacts with the Forkhead Box-O transcription factor gene, *dFOXO,* via the Insulin/Insulin-like Receptor (InR) and c-Jun N-terminal Kinase (JNK) pathways to regulate interommatidial bristle formation. First, we plan to characterize the genetic interaction of *mid* with *dFOXO* and members of the InR and JNK pathways using genetic

and allelic modifier screens. Since *dFOXO* is a key regulator of stress responses, we aim to elucidate *mid*'s role in regulating cell survival under conditions of physiological stress by inducing oxidative and nutritional stress within wild-type and *mid* mutant larvae. Finally, we will investigate whether Mid and its paralog, H15, are detected within the nucleus and cytoplasm. Toward this goal, we will utilize the Western blot assay to probe for Mid and H15 within the nucleus and cytoplasm of wild-type and *mid* mutant larvae.

CHAPTER II

METHODOLOGY

Fly Stocks

Drosophila melanogaster strains were maintained at 25^{o}C on standard cornmeal-yeast-agar media on a 12 hour light-dark cycle. *Oregon-R* flies were used as wild-type (WT) and the *yw;+/+;FRT82dFOXO^{25}/TM6 Tb Hu* line was provided by Ernst Hafen (Junger et al., 2003) (Figure 7) (Tables 1 & 2). We used the *UAS-Gal4* system (Brand and Perrimon, 1993) and the eye-specific driver *GMR-Gal4* balanced on chromosome III (a gift from Tanya Wolff; Hay et al., 1994) to express *UAS-mid-RNAi* in WT and specific mutant backgrounds (provided by Rolf Bodmer) (Qian et al., 2005).

The *GFP-dFOXO* transgenic line *w^{1118};P{GMR59G09-GAL4}attP2* and the following lines were obtained from the Bloomington Stock Center (Bloomington, Indiana): *Df(3R)ED5634* (stock 9228), *Df(3R)Exel7321* (stock 7977), *Df(3R)BSC617* (stock 25692), and *Df(3R)BSC470* (stock 24974) (Table 3). Except where noted, all of the following stocks of mutant alleles listed in Table 1 were also obtained from the Bloomington Stock Center (IN).

Table 1

Comprehensive list of all stocks tested

Stock Number	Abbreviated Genotype	Genotype	Representation	Statistical Value for *mid-RNAi* Suppression
18479	*CG9922^{f01836}*	*w^{1118};PBac{WH}CG9922^{f01836}/TM6B, Tb^{1}*	Table 2	*p* = 0.0211 Wilcoxon
21288	*CG3061^{DG25606}*	*y^{1}w^{67c23};P{wHy}CG3061^{DG25606}*	Table 2	*p* = 0.5718 Wilcoxon
24694	*Npc2b^{MB04347}*	*w^{1118};Mi{ET1}Npc2b^{MB04347}*	Table 2	*p* = 0.0493 Wilcoxon
18464	*PK1-R^{f01726}*	*w^{1118};PBac{WH}PK1-R^{f01726}*	Table 2	*p* = 0.0070 ANOVA
29266	*CCHa1^{MB11962}*	*w^{1118};Mi{ET1}CCHa1^{MB11962}*	Table 2	*p* = 0.0006 ANOVA
12138*	*Cyp6d5 - RNAi*	*w^{1118};P{GD2979}v12138*	Table 2	*p* = 0.5778 ANOVA
44657	*CG9920 - RNAi*	*y^{1}sc*v^{1};P{TRiP.HMC02438}attP2*	Table 2	*p* = 0.0309 Wilcoxon
20323	*rdx^{EY11582}*	*y^{1}w^{67c23};P{EPgy2}rdx^{EY11582}*	Table 2	*p* = 0.0066 ANOVA
32475	*dIlp2 - RNAi*	*y^{1}sc*v^{1};P{TRiP.HMS00476}attP2/TM3, Sb^{1}*	-----	*p* = 0.0640 Wilcoxon
30881	*dIlp2^{1}*	*w^{1118};Ilp2^{1}*	Fig. 3A,Table 3	*p* = 0.0029 ANOVA
31068	*dIlp2 - RNAi*	*y^{1}v^{1};P{TRiP.JF01518}attP2*	-----	*p* = 0.6775 Wilcoxon
30884	*dIlp5^{1}*	*w^{1118};Ilp5^{1}*	-----	*p* = 0.0080 ANOVA
31378	*dIlp5 - RNAi*	*y^{1}v^{1};P{TRiP.JF01347}attP2*	Fig. 3B,Table 3	*p* = 0.0002 Wilcoxon
31379	*dIlp6 - RNAi*	*y^{1}v^{1};P{TRiP.JF01347}attP2*	Fig. 3C,Table 3	*p* < 0.0001 ANOVA
33684	*dIlp6 - RNAi*	*y^{1}sc*v^{1};P{TRiP.HMS00549}attP2*	-----	*p* = 0.1565 ANOVA
51518	*dInR - RNAi*	*y^{1}v^{1};P{TRiP.HMS03166}attP40*	-----	*p* = 0.0411 Wilcoxon
9646	*InR^{E19}*	*InR^{E19}/TM2*	Fig. 3D,Table 3	*p* = 0.0091 Wilcoxon
9554	*InR^{93D}-4*	*In(3R)GC25,InR^{93D}-4/TM3, Sb^{1}*	-----	*p* = 0.7912 Wilcoxon
10738	*chico^{1}*	*cn^{1}P{ry11}chico^{1}/CyO;ry^{506}*	-----	*p* = 0.8798 Wilcoxon
36665	*chico - RNAi*	*y^{1}v^{1};P{TRiP.HMS01553}AttP2/TM3,Sb^{1}*	Fig. 3E,Table 3	*p* = 0.0058 Wilcoxon
18214	*Pi3K59F^{e03961}*	*w^{1118};PBac{RB}Pi3K59F^{e03961}*	-----	*p* = 0.7913 Wilcoxon
31252	*Pi3K68D - RNAi*	*y^{1}v^{1};P{TRiP.JF01193}attP2*	Fig. 3F,Table 3	*p* < 0.0001 ANOVA
28473	*Pi3K59F^{EG6017}*	*y^{1}w*;p{EP}Pi3K59F^{EG6017}*	-----	*p* < 0.0001 ANOVA
27725	*Pdk1 - RNAi*	*y^{1}v^{1}:P{TRiP.JF02807}attP2*	-----	*p* = 0.9698 Wilcoxon
25841	*PTEN - RNAi*	*y^{1}v^{1};P{TRiP.JF01859}attP2*	-----	*p* = 0.7336 Wilcoxon
33643	*PTEN - RNAi*	*y^{1}v^{1};P{TRiP.HMS00044}attP2*	Fig. 3GTable 3	*p* < 0.0001 ANOVA
25967	*PTEN - RNAi*	*y^{1}v^{1};P{TRiP.JF01987}attP2*	-----	*p* = 0.0005 Wilcoxon
11627	*Akt1^{04226}*	*ry^{506}P{PZ}Akt1^{04226}/TM3, ry^{RK} Sb^{1} Ser^{1}*	Fig. 3H,Table 3	*p* = 0.0172 Wilcoxon
31701	*Akt1 - RNAi*	*y^{1}v^{1};P{TRiP.HM04007}attP2*	-----	*p* = 0.2725 Wilcoxon
11218	*Tor^{k17004}*	*y^{1}w^{67c23};P{lacW}Tor^{k17004}/CyO*	Fig. 3J,Table 3	*p* = 0.0002 Wilcoxon
35578	*Tor - RNAi*	*y^{1}sc^{v1};P{TRiP.GL00156}attP2*	-----	*p* = 0.0411 Wilcoxon
9559	*Thor^{2}*	*y^{1}w*;Thor^{2}*	-----	*p* = 0.2892 Wilcoxon
36815	*Thor - RNAi*	*y^{1}sc*v^{1};P{TRiP.GL01034}attP2*	-----	*p* = 0.6793 ANOVA
21215	*dfoxo^{EY16506}*	*y^{1}w^{67c23};P{w[=mC]y[+mDint2]=EPgy2}foxo^{EY16506}*	Fig. 2,Table 3	*p* = 0.0002 Wilcoxon
42220	*dfoxo$^{\Delta 94}$*	*dfoxo$^{\Delta 94}$/TM6B, Tb^{1}*	Fig. 3I,Table 3	*p* = 0.0002 Wilcoxon
**	*dfoxo^{25}*	*yw;FRT82dfoxo^{25}/TM6B, Tb^{1}H*	Whole: Fig. 2G,Table 1 Dorsal: Table 2	*p* = 0.0002 Wilcoxon *p* < 0.0001 ANOVA
41605	*slpr - RNAi*	*y^{1}v^{1};P{TRiP.GL01187}attP2*	-----	*p* = 0.2896 Wilcoxon
32948	*slpr - RNAi*	*y^{1}sc*v^{1};P{TRiP.HMS00742}attP2*	Fig. 4A,Table 4	*p* = 0.0014 ANOVA
35210	*hep - RNAi*	*y^{1}sc*v^{1};P{TRiP.GL00089}attP2*	-----	*p* = 0.0311 Wilcoxon
28710	*hep - RNAi*	*y^{1}v^{1};P{TRiP.JF03137}*	Fig. 4B,Table 4	*p* = 0.0001 ANOVA
28927	*Cka - RNAi*	*y^{1}v^{1};P{TRiP.HM05138}*	Fig. 4C,Table 4	*p* = 0.0002 Wilcoxon
31642	*Cka - RNAi*	*y^{1}v^{1};P{TRiP.JF01432}*	-----	*p* = 0.0889 Wilcoxon
32977	*bsk - RNAi*	*y^{1}sc*v^{1};P{TRiP.HMS00777}attP2*	-----	*p* = 0.1019 ANOVA
31476	*bsk - RNAi*	*y^{1}v^{1};P{TRiP.JF01274}attP2*	Fig. 4D,Table 4	*p* < 0.0001 ANOVA
3088	*bsk^{1}*	*bsk^{1}cn^{1}bw^{1}sp^{1}/CyO*	-----	*p* = 0.2261 Wilcoxon
31595	*djun - RNAi*	*y^{1}v^{1};P{TRiP.JF01184}*	Fig. 4E,Table 4	*p* = 0.0002 Wilcoxon
31322	*dfos - RNAi*	*y^{1}v^{1};P{TRiP.JF01273}*	-----	*p* = 0.0639 Wilcoxon
27722	*dfos - RNAi*	*y^{1}v^{1};P{TRiP.JF02804}*	Fig. 4F,Table 4	*p* < 0.0001 ANOVA
23695	*puc^{67BDn}*	*ru^{1}puc^{67BDn}red^{1}e^{1}/TM3, Sb^{1}*	Fig. 4G,Table 4	*p* = 0.0028 Wilcoxon
34392	*puc - RNAi*	*y^{1}sc*v^{1};P{TRiP.HMS01386}attP2*	-----	*p* = 0.9999 ANOVA

Note. A single asterisk indicates a stock obtained from the Vienna *Drosophila* Resource Center. A double asterisk indicates a stock received from Ernst Hafen.

Collecting Eye Images for Genetic and Allelic Modifier Screens

We screened a fraction of isogenized DrosDel deficiency lines obtained from the Bloomington Stock Center by crossing each line to *UAS-mid-RNAi/CyO*;*GMR-Gal4*/*TM3* (*mid-RNAi*) flies exhibiting a sensitized genetic mutation for *mid* characterized by an approximate 50% decrease of bristle complexes (Das et al., 2013). Bristles were counted from one-day old female progeny generated from the cross that were maintained at 25ºC. Groups of ten flies of the genotype *UAS-mid-RNAi/+;GMR-Gal4/Df(3)* or *UAS-mid-RNAi/+;GMR-Gal4/allele* (as well as other progeny of select genotypes) were transfixed to a slide with clear nail polish lacquer and submerged in water. The complete eye field was viewed under a high-power Leica M165C dissection microscope. A series of images were collected along 10-15 focal planes and digitally recorded using a Leica DFC camera. These images were flattened to create a final montage using Image Pro Plus software to correct for eye curvature and to digitally tag bristles within the dorsal half of the eye for accurate quantification (Media Cybernetics Inc., Bethesda, MD). Using these methods, we identified several deficiency lines that modified the *mid* mutant phenotype (unpublished data). Of these lines, flies heterozygous for *Df(3R)ED5634* (88A4;88B1) placed within the *mid*-RNAi genetic background significantly suppressed the *mid* mutant phenotype. Overlapping deficiency analyses were carried out and the outcome is reported in the results section as well as in Figure 8 and Table 3.

Oxidative Stress Studies

WT OR and *mid-RNAi* flies were maintained in population cages and allowed to lay eggs for 4 hours on 150 mm apple-juice caps with yeast paste. After 4 hours, the plates were removed and lightly watered every day until the eggs developed into three-

day old 3ºL. The 3ºL were starved for 6 hours and then transferred to vials with 1% agar in ddH_2O and 0.5% yeast paste mixed with or without paraquat until larvae transitioned into pupae. The doses of paraquat tested were 1, 5, 10, 20, and 30 mM. After eclosion, 30 treated and nontreated one-day old female flies were exposed to Flynap (Carolina Biologicals) for anesthesia, collected, and mounted with nail polish on a glass slide for gathering eye images as previously described. Paraquat was obtained from Sigma Aldrich (St. Louis, MO).

Metabolic Stress Studies

WT OR and *UAS-mid-RNAi/CyO;GMR-Gal-4/TM3* flies were maintained in population cages and then allowed to lay eggs for 4 hours on grape juice caps with yeast paste. Approximately 80 hours after egg laying, 3ºL larvae were transferred into vials with either standard fly medium or starvation medium (8% agar in PBS) for 24 hours. *UAS-mid-RNAi* flies were transferred to media conditions after 88 hours due to a slight delay of their growth. After 24 hours, 30 flies were collected and dorsal ommatidial bristles were scored using a Leica DFC295 light microscope with Image-Pro Analyzer 7.0 software (Media Cybernetics). Ommatidial areas were measured using ImageJ (NIH).

Purification of Nuclear and Cytoplasmic Extracts

We followed the protocol of Udvardy and Schedyl (1984) with only slight modifications to obtain relatively pure nuclear and cytoplasmic fractions. Approximately 0.5 gm (~500 µl wet volume) of WT, *mid-RNAi,* and $dFOXO^{\Delta 94}$ 3ºL were collected and snap frozen under liquid nitrogen for storage. Frozen 3ºL larvae were pulverized under liquid nitrogen with a mortar and pestle and dounce homogenized on ice in cold "Buffer A" containing 0.25M sucrose, 60 mM KCl, 15 mM NaCl, 15 mM Tris-HCl (pH = 7.5),

0.1 mM EGTA, 1 mM EDTA, 1mM dithiothreitol, aprotonin (2 µg/ml), and leupeptin (0.5 µg/ml). The homogenate was spun at 5,000 RPM (3,024 x g) using the JA-20 rotor for 5 minutes to remove debris. NP-40 was then added to a final v/v concentration of 0.2% followed by a short 5 second vortex and three 10 second high-frequency pulses on ice using a Fisher sonic dismembrator model 300. The nuclei were pelleted at 5,000 RPM for 10 minutes using the JA-20 and the cytoplasmic extract was isolated (supernatant). The nuclear pellets were resuspended in "Buffer A*" without EDTA and EGTA, but supplemented with 1 mM $CaCl_2$. The nuclei were spun again at 5,000 RPM for 10 minutes and resuspended in "Buffer A*". We validated that nuclei were isolated using the trypan blue exclusion test and observing the extract under a high-magnification compound light microscope. Cytoplasmic and nuclear extracts were flash frozen in liquid nitrogen and stored at -70^{o}C until further use. All chemicals used were obtained from Sigma-Aldrich (St. Louis, MO).

Western Analyses

We used the Bradford assay (Pierce Biochemical) to measure protein concentrations of nuclear and cytoplasmic fractions for loading equivalent sample amounts for SDS-PAGE. We ran the samples on either a 4-15% gradient gel (Bio-Rad) or a 10% gel and then transferred the proteins to a polyvinylidene difluoride (PVDF) membrane for immunoblotting with rabbit anti-Mid antibody at a 1:1000 dilution (Leal et al., 2009), guinea-pig anti-H15 antibody at a 1:5000 dilution (Leal et al., 2009), mouse anti-LaminC antibody at a 1:1000 dilution (Developmental Studies Hybridoma Bank, Iowa, WI), or mouse anti-tubulin antibody at 1:333 dilution (Developmental Studies Hybridoma Bank, Iowa, WI) for 4 hours at 25^{o}C in PBST (PBS containing 0.1% Tween)

containing 5% milk (Carnation®) followed by three 10 minute rinses with PBST. The PVDF membrane was next incubated with secondary anti-rabbit, anti-guinea pig, or anti-mouse antibodies conjugated to horse radish peroxidase at a dilution of 1:30,000 for 1 hr at 25^{o}C. Following this incubation and three 5 minute washes with PBST, we used the Amersham ECL Prime Western Blotting Detection Reagent from GE Healthcare to develop the immunoblot. We also carried out either Coomassie Blue or Ponceau-S staining of the PVDF membrane after the protein transfer to check for equivalent loading of proteins.

Statistical Analyses

The mean and standard errors of the mean were calculated using Microsoft Excel software. The IOB counts for each genotype were statistically analyzed using Shaprio-Wilk's test for measuring the normal distribution of each data set (JMP10 software, SAS Institute Inc.). We also estimated the equal variance between groups using the Barlett's test. Data sets that met the assumptions of a normal distribution and equal variance were then analyzed using the one-factor ANOVA and Tukey's HSD to generate *p* values between assessed pairs of data. Data sets exhibiting unequal variance or an unequal distribution were analyzed by the Wilcoxon rank-sum test. All of the probability values were calculated setting the level of significance (α) to 0.05.

Software Programs

Confocal images were assembled using Adobe Photoshop CS6 software (Adobe Systems, Inc.). We used GraphPad Software, Inc. (La Jolla, CA) to present data in bar chart format. Image J (NIH) was used to measure the surface area of compound eyes.

CHAPTER III

RESULTS

A Genetic Modifier Screen Identifies *dFOXO* and Novel Gene Candidates that Interact with *mid*

We combined the *UAS-Gal4* binary expression system (Brand & Perrimon, 1993) with RNAi methodology (Lee & Carthew, 2003) to generate a perpetual line of *UAS-mid-RNAi;GMR-Gal4* (*mid-RNAi*) mutant flies. The *GMR-Gal4* driver targets the reduction of *mid* within and posterior of the morphogenetic furrow (MF) in the eye imaginal disc of 3^{o}L. The MF is a contractile wave of differentiating tissue from which precursor cells are recruited in stepwise fashion to form clusters of cells that will develop into ommatidia, the unit facets of the adult eye. One-day old female *mid-RNAi* mutant flies exhibit compound eyes characterized by an approximate 50% loss of interommatidial bristles (IOBs), ommatidial fusion, reduced pigmentation, and cell death (Figure 7B) (Das et al., 2013).

From a genetic modifier screen, we found that placing the *Dros Del* chromosomal deficiency line *Df(3R)ED5634* in a heterozygous mutant state within the *UAS-mid-RNAi;GMR-Gal4* background suppressed the *mid-RNAi* mutant phenotype. *UAS-mid-RNAi/+;GMR-Gal4/Df(3R)ED5634* progeny exhibited an ~20% loss of bristles compared to the ~58% loss observed in *mid-RNAi* progeny (Figure 7C) (Table 2). F1 progeny carrying either the *UAS-mid-RNAi*, *GMR-Gal4* transgenes or the heterozygous *Df(3R)ED5634* deficiency alone expressed normal numbers of IOBs approximating those quantitated for wild-type (WT), Oregon-R (OR) flies (Figure 7D) (Table 2).

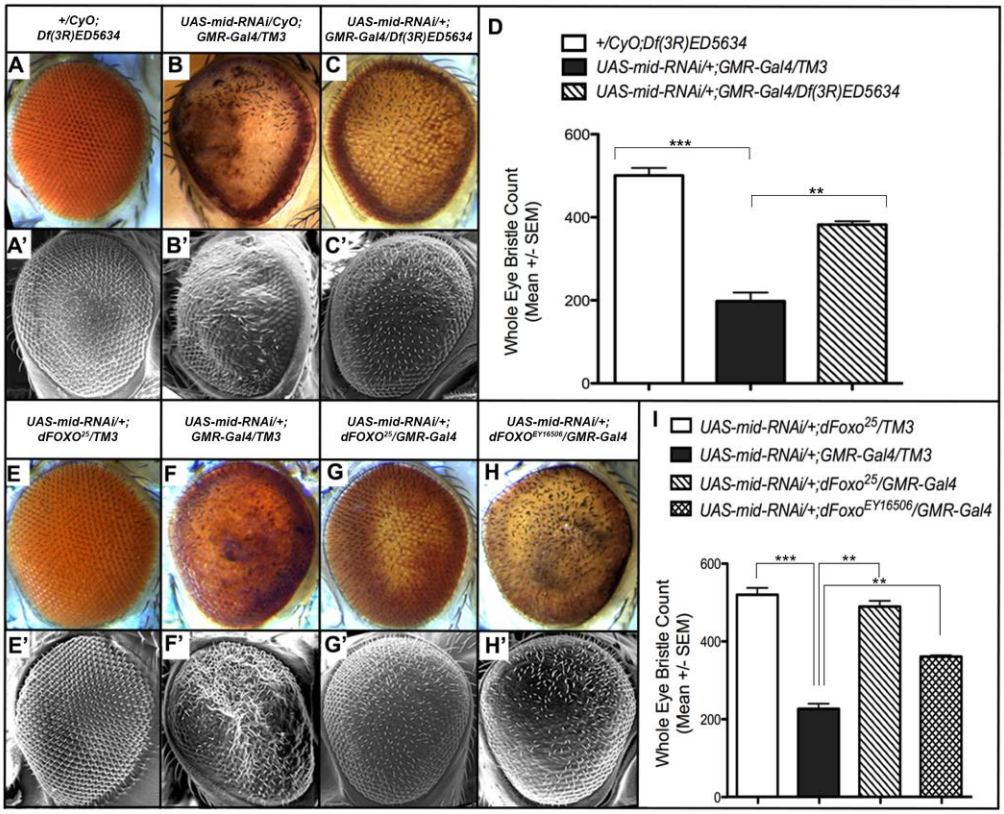

Figure 7. dFOXO collaborates with Mid to regulate SOP formation and survival. (A) WT and (B) *mid*-RNAi compound eyes exhibit features previously described in Das et al. (2013). The WT eye displays a uniform ommatidial array while the *mid-RNAi* eye is grossly deformed with cell fusion, reduced pigmentation, and a significant loss of IOBs. (C) Placing *mid*-RNAi in a heterozygous *Df(3R)ED5634* background suppresses the mutant phenotype with a partial recovery of bristles. (D) The bar chart represents mean bristle numbers +/- SEM quantitated for 10 eyes per experimental group. Statistical analyses indicates a significant decrease in bristle numbers within *mid*-RNAi eyes and a significant recovery of bristles in *UAS-mid-RNAi/+GMR-Gal4/Df(3R)ED5634* eyes. (E) An internal control generated from the cross of the genotype *UAS-mid-RNAi/+;FRT82dFOXO^{25}/TM3* is represented. (F) A *mid-RNAi* compound eye generated from a progeny of the cross depicts a significant loss of interommatidial bristles. (G) Placing *mid-RNAi* flies in a heterozygous *dFOXO^{25}* background significantly suppresses the mutant phenotype (p*=0.0002). (H) Placing *mid-RNAi* flies in a heterozygous *dFOXO^{EY16506}* background partially suppresses the mutant phenotype (p**=0.0002). (I) The bar chart shows the mean bristle numbers and SEM for eyes from ten flies of the genotypes shown in panels E-H. (A'-C') and (E'-H') are scanning electron microscope images of replicate compound eyes showing the WT and mutant bristle phenotypes. Comparisons of data represented by bar charts are indicated by *brackets* linking specific data sets. The values represented in the bar charts shown in panels (D) and (I) are reported within Table 1, respectively, in addition to statistical data with p-value parameters. Other genotypes of progeny generated from parental crosses were phenotypically WT (data not shown).

Table 2

Comparisons of whole eye IOB mean counts of dFOXO mutant alleles and the deficiency line Df(3R)ED5634

ED5634	UAS-mid-RNAi/+;TM3/ Df(3R)ED5634	CyO/+; TM3/Df(3R)ED5634	CyO/+;GMR-Gal4/ Df(3R)ED5634	UAS-mid-RNAi/+; GMR-Gal4/TM6	UAS-mid-RNAi/+; GMR-Gal4/ Df(3R)ED5634	% Recovery	*p*-value
	500±18	583±19	468±12	198±20	383±8	93%	*p*=0.0002
dFOXO	UAS-mid-RNAi/+;TM3/ FRT82.dFOXO^{25}	CyO/+; TM3/FRT82.dFOXO^{25}	CyO/+;GMR-Gal4/ FRT82.dFOXO^{25}	UAS-mid-RNAi/CyO; GMR-Gal4/TM6.Sb	UAS-mid-RNAi/+; GMR-Gal4/ FRT82.dFOXO^{25}	% Recovery	*p*-value
	520±18	573±7	571±11	227±13	490±15	115%	*p*=0.0002
dFOXO	UAS-mid-RNAi/ dFOXO^{EY16506};TM3/+	CyO/+; TM3/dFOXO^{EY16506}	CyO/+;GMR-Gal4/ dFOXO^{EY16506}	UAS-mid-RNAi/CyO; GMR-Gal4/TM3	UAS-mid-RNAi/ dFOXO^{EY16506}; GMR-Gal4/+	% Recovery	*p*-value
	585±14	536±15	474±14	228±11	361±3	58%	*p*=0.0002

Note. Each column represents a specific genotype and the mean whole eye IOB count +/- SEM. The first two uncolored columns are additional F1 progeny recovered in the genetic modifier screens which do not carry the *GMR-Gal4* driver line. The green, red, and blue labeled columns correspond to the similarly labeled genotypes shown in Figure 2. Recovery was determined as the percentage change between the flies with the *mid-RNAi* condition (red column) and flies with a heterozygous deficiency interval or mutant allele in the background of the *mid-RNAi* condition (blue column). The data sets represented in the bar graph were statistically analyzed using tests as described in detail in section 4.9 of the methods.

Df(3R)ED5634 deletes the cytological region 88A4-88B1. We initiated overlapping chromosomal deficiency mapping to further delimit the cytological interval harboring *mid*-interacting genes. *Df(3R)BSC617* deletes cytological interval 88A8-88B1 which partially overlaps with 88A4-88B1 (Table 3). We found that one-day old adult *UAS-mid-RNAi/+;GMR-Gal4/BSC617* flies did not suppress the *mid-RNAi* mutant bristle phenotype (Table 3). We next validated this result by generating *UAS-mid-RNAi/+;GMR-Gal4/Df(3R)Exel7321* flies where *Df(3R)Exel7321* deletes the cytological region 88A9-88B1 (Figure 8). Since the bristle numbers of *UAS-mid-RNAi/+;GMR-Gal4/Df(3R)Exel7321* eyes again recapitulated the *mid-RNAi* mutant phenotype, we were able to delimit the chromosomal interval harboring *mid*-interacting genes to 88A4-88A8

with confidence (Table 3). We also generated *UAS-mid-RNAi/+;GMR-Gal4/Df(3R)BSC470* flies. The *Df(3R)BSC470* line deletes region 88A11 to 88B1 (Figure 8). The bristle numbers of *UAS-mid-RNAi/+;GMR-Gal4/Df(3R)BSC470* also recapitulated the *mid-RNAi* phenotype (Table 3).

Table 3

Dorsal IOB counts for chromosomal deficiency lines

ED5634	UAS-mid-RNAi/+;TM3/ Df(3R)ED5634	CyO/+; TM3/Df(3R)ED5634	CyO/+;GMR-Gal4/ Df(3R)ED5634	UAS-mid-RNAi/+; GMR-Gal4/ TM6C,Sb',cu'	UAS-mid-RNAi/+; GMR-Gal4/ Df(3R)ED5634	% Recovery	*p*-value
	289±8	252±8	247±6	126±22	183±12	46%	*p*=0.0452
BSC617	UAS-mid-RNAi/+;TM3/ Df(3R)BSC617	CyO/+; TM3/Df(3R)BSC617	CyO/+;GMR-Gal4/ Df(3R)BSC617	UAS-mid-RNAi/CyO; GMR-Gal4/ TM6C,Sb',cu'	UAS-mid-RNAi/+; GMR-Gal4/ Df(3R)BSC617	% Recovery	*p*-value
	322±5	290±4	274±5	210±6	227±6	8%	*p*=0.7052
Exel7321	UAS-mid-RNAi/+;TM3/ Df(3R)Exel7321	CyO/+; TM3/Df(3R)Exel7321	CyO/+;GMR-Gal4/ Df(3R)Exel7321	UAS-mid-RNAi/CyO; GMR-Gal4/TM6B,Tb'	UAS-mid-RNAi/+; GMR-Gal4/ Df(3R)Exel7321	% Recovery	*p*-value
	312±7	287±11	278±2	205±16	219±7	7%	*p*=0.7910
BSC470	UAS-mid-RNAi/+;TM3/ Df(3R)BSC470	CyO/+; TM3/Df(3R)BSC470	CyO/+;GMR-Gal4/ Df(3R)BSC470	UAS-mid-RNAi/CyO; GMR-Gal4/ TM6C,Sb',cu'	UAS-mid-RNAi/+; GMR-Gal4/ Df(3R)BSC470	% Recovery	*p*-value
	302±9	270±7	273±14	233±27	255±15	9%	*p*=0.9397

Note. Each column represents a specific genotype and the mean dorsal IOB count +/- SEM. The first two uncolored columns are additional F1 progeny recovered in the genetic modifier screens which do not carry the *GMR-Gal4* driver line. The green-labeled genotype represents an F1 progeny heterozygous for both the mutant allele and the GMR-Gal4 driver line which provides a WT phenotype of bristle numbers that are nearly equivalent to those of OR flies. The red-labeled genotype represents an F1 progeny designated as a *mid-RNAi* condition except where there is a "P". The "P" label indicates that an internal F1 *mid-RNAi* genotype was not generated from the cross and the genotype represents a parental *mid-RNAi* compound eye (*UAS-mid-RNAi/CyO;GMR-Gal4/TM3*). The blue-labeled genotype represents an F1 progeny that places a heterozygous mutant allele or *UAS-RNAi-TRiP* line of an InR pathway member in a *mid-RNAi* background to assay for enhancement or suppression of the *mid-RNAi* phenotype. Recovery was determined as the percentage change between the flies with the *mid-RNAi* condition (red column) and flies with a heterozygous mutant allele in the background of the *mid-RNAi* condition (blue column). The data sets represented in the bar graph were statistically analyzed using tests as described in detail in section 4.9 of the methods.

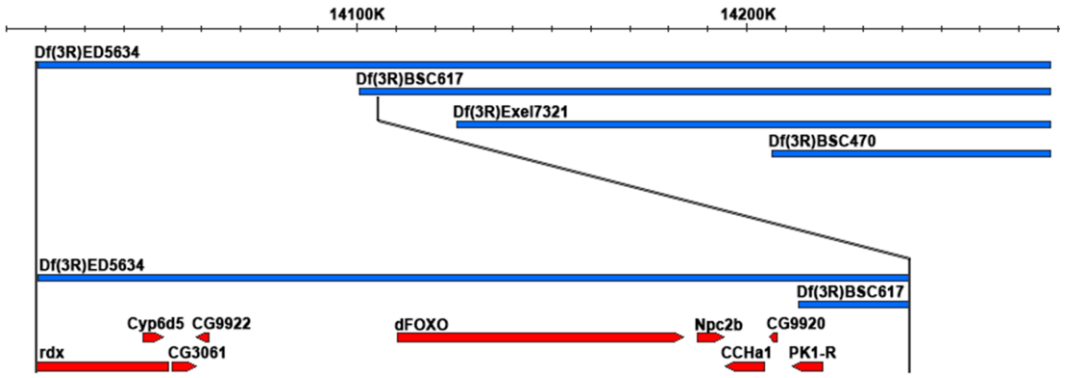

Figure 8. Chromosomal deficiency mapping analyses narrow the cytological region harboring mid-interacting genes. The cartoon illustrates the mapping analyses carried out by crossing overlapping deficiency lines with the *mid-RNAi* line. The cartoon was adapted from a schematic illustrated in GBrowse (Flybase.org). The endpoints of the delimited region harboring *mid* interacting genes are 3R:14,017.903..14,100.457 (Cytological region 88A4-88A8).

The 88A4-88A8 region deletes the following genes listed in the order of their reported loci within the genome (Flybase.org): *roadkill* (*rdx*), *Cyp6d5*, *CG3061*, *CG9922*, *dFOXO*, *Npc2b*, *CCHa1*, *CG9920*, and *pk1r* (Figure 8). We placed a null mutant allele and/or transgenic RNAi line of each gene within the *mid-RNAi* background to identify potential *mid*-interacting genes by screening for suppressors of the *mid-RNAi* phenotype. We found that placing mutations of *rdx*, *Cyp6d5*, *CG9922*, *dFOXO*, and *pkr1* in the *mid-RNAi* background significantly suppressed the *mid-RNAi* mutant phenotype (Table 4). IOBs were recovered and tissue integrity was partially recovered (data not shown).

As discussed, *dFOXO* functions downstream of the InR and JNK signaling pathways. We decided to pursue the functional characterization of *dFOXO* as a *mid*-interacting gene to elucidate the *mid*-specific transcription factor regulatory network guiding the specification of cells as well as promoting their survival. The latter relationship associating a novel survival function for *mid* has only been reported for one T-box gene, *T-bet*. The *T-bet* gene has been shown to regulate cytokine production under

conditions of stress in differentiating T-helper cells within the immune system of the mouse (Rockwell, Zhang, Fields, & Klaassen, 2012; Szabo et al., 2000).

We first placed a heterozygous mutant allele of *dFOXO*, $dFOXO^{25}$, in the *mid*-RNAi background to determine whether *UAS-mid-RNAi/+;GMR-Gal4/*$dFOXO^{25}$ flies recapitulated the suppression of the mutant eye bristle phenotype observed in *UAS-mid-RNAi/+;GMR-Gal4/Df(3R)ED5634* flies. We found that bristles were significantly increased in *UAS-mid-RNAi/+;GMR-Gal4/*$dFOXO^{25}$ adult eyes (Figure 7G, I) (Table 2). The deposition of pigment was also recovered throughout the adult eyes of *UAS-mid-RNAi/+;GMR-Gal4/*$dFOXO^{25}$ flies (Figure 6G). We next placed a semi-lethal mutant allele of *dFOXO* in the *mid*-RNAi background designated $dFOXO^{EY16506}$. The $dFOXO^{EY16506}$ line is one of several enhancer trap lines designed to track the *dFOXO* expression pattern using a surrogate *B-galactosidase* reporter gene inserted downstream from the *dFOXO* enhancer region. The $dFOXO^{EY16506}$ P-element insertion is also located approximately 18 kb downstream from the *dFOXO* promoter region before the coding region for the *dFOXO* transcription factor DNA-binding motif. Placing $dFOXO^{EY16506}$ in a heterozygous state in the *mid*-RNAi background partially recovered bristles (Figure 7H, I) (Table 2) indicating that the C-terminal domain of the dFOXO protein expressed from the $dFOXO^{EY16506}$ mutant allele retained partial functional activity. These results identify *dFOXO* as a novel and specific *mid*-interacting gene.

Table 4

Dorsal mean IOB counts of mid-interacting candidate genes identified from a genetic modifier screen

rdx	*UAS-mid-RNAi/+;TM3/ P{EPgy2}rdx^{EY11582}*	*CyO/+;TM3/ P{EPgy2}rdx^{EY11582}*	*CyO/+;GMR-Gal4/ P{EPgy2}rdx^{EY11582}*	P *UAS-mid-RNAi/CyO; GMR-Gal4/TM3*	*UAS-mid-RNAi/+; GMR-Gal4/ P{EPgy2}rdx^{EY11582}*	% Recovery	*p*-value
	330±13	325±6	283±6	181±12	230±11	27%	*p*=0.0066
Cyp6d5	*UAS-mid-RNAi/+;TM3/ P{GD2979}v12138*	*CyO/+;TM3/ P{GD2979}v12138*	*CyO/+;GMR-Gal4/ P{GD2979}v12138*	P *UAS-mid-RNAi/CyO; GMR-Gal4/TM3*	*UAS-mid-RNAi/+; GMR-Gal4/ P{GD2979}v12138*	% Recovery	*p*-value
	323±8	315±6	313±10	181±12	201±12	11%	*p*=0.5778
CG3061	*UAS-mid-RNAi/+;TM3/ P{wHy}CG3061^{DG25606}*	*CyO/+;TM3/ P{wHy}CG3061^{DG25606}*	*CyO/+;GMR-Gal4/ P{wHy}CG3061^{DG25606}*	*UAS-mid-RNAi/CyO; GMR-Gal4/TM3*	*UAS-mid-RNAi/+; GMR-Gal4/ P{wHy}CG3061^{DG25606}*	% Recovery	*p*-value
	346±8	315±6	281±8	182±17	180±8	-1%	*p*=0.5718
CG9922	*UAS-mid-RNAi/+;TM3/ PBac{WH}CG9922^{f01835}*	*CyO/+;TM3/ PBac{WH}CG9922^{f01835}*	*CyO/+;GMR-Gal4/ PBac{WH}CG9922^{f01835}*	*UAS-mid-RNAi/CyO; GMR-Gal4/TM6B,Tb^{1}*	*UAS-mid-RNAi/+; GMR-Gal4/ PBac{WH}CG9922^{f01835}*	% Recovery	*p*-value
	323±7	301±7	270±7	167±15	215±14	29%	*p*=0.0211
dFOXO	*UAS-mid-RNAi/+;TM3/ FRT82.dFOXO^{25}*	*CyO/+;TM3/ FRT82.dFOXO^{25}*	*CyO/+;GMR-Gal4/ FRT82.dFOXO^{25}*	*UAS-mid-RNAi/CyO; GMR-Gal4/ TM6B.Tb.Hu*	*UAS-mid-RNAi/+; GMR-Gal4/ FRT82.dFOXO^{25}*	% Recovery	*p*-value
	342±8	294±6	266±4	189±7	278±6	47%	*p*<0.0001
Npc2b	*UAS-mid-RNAi/+;TM3/ Mi{ET1}Npc2b^{MB04347}*	*CyO/+;TM3/ Mi{ET1}Npc2b^{MB04347}*	*CyO/+;GMR-Gal4/ Mi{ET1}Npc2b^{MB04347}*	*UAS-mid-RNAi/+; GMR-Gal4/TM3.Sb*	*UAS-mid-RNAi/+; GMR-Gal4/ Mi{ET1}Npc2b^{MB04347}*	% Recovery	*p*-value
	333±5	291±8	268±4	179±16	222±7	24%	*p*=0.0493
CCHa1	*UAS-mid-RNAi/+;TM3/ Mi{ET1}CCHa1^{MB11962}*	*CyO/+;TM3/ Mi{ET1}CCHa1^{MB11962}*	*CyO/+;GMR-Gal4/ Mi{ET1}CCHa1^{MB11962}*	*UAS-mid-RNAi/CyO; GMR-Gal4/TM3*	*UAS-mid-RNAi/+; GMR-Gal4/ Mi{ET1}CCHa1^{MB11962}*	% Recovery	*p*-value
	326±6	302±8	289±8	187±10	249±14	33%	*p*=0.0006
CG9920	*UAS-mid-RNAi/+;TM3/ P{TRiP.HMC02438}attP2*	*CyO/+;TM3/ P{TRiP.HMC02438}attP2*	*CyO/+;GMR-Gal4/ P{TRiP.HMC02438}attP2*	P *UAS-mid-RNAi/CyO; GMR-Gal4/TM3*	*UAS-mid-RNAi/+; GMR-Gal4/ P{TRiP.HMC02438}attP2*	% Recovery	*p*-value
	320±9	288±6	261±6	181±12	226±11	25%	*p*=0.0309
PK1R	*UAS-mid-RNAi/+;TM3/ PBac{WH}PK1-R^{f01726}*	*CyO/+;TM3/ PBac{WH}PK1-R^{f01726}*	*CyO/+;GMR-Gal4/ PBac{WH}PK1-R^{f01726}*	P *UAS-mid-RNAi/CyO; GMR-Gal4/TM3*	*UAS-mid-RNAi/+; GMR-Gal4/ PBac{WH}PK1-R^{f01726}*	% Recovery	*p*-value
	327±8	310±7	301±7	181±12	222±6	23%	*p*=0.0070

Note. Each column represents a specific genotype and the mean dorsal IOB count +/- SEM. The first two uncolored columns are additional F1 progeny recovered in the genetic modifier screens which do not carry the *GMR-Gal4* driver line. The green-labeled genotype represents an F1 progeny heterozygous for both the mutant allele and the GMR-Gal4 driver line which provides a WT phenotype of bristle numbers that are nearly equivalent to those of OR flies. The red-labeled genotype represents an F1 progeny designated as a *mid-RNAi* condition except where there is a "P". The "P" label indicates that an internal F1 *mid-RNAi* genotype was not generated from the cross and the genotype represents a parental *mid-RNAi* compound eye (*UAS-mid-RNAi/CyO;GMR-Gal4/TM3*).

The blue-labeled genotype represents an F1 progeny that places a heterozygous mutant allele or *UAS-RNAi-TRiP* line of an InR pathway member in a *mid-RNAi* background to assay for enhancement or suppression of the *mid-RNAi* phenotype. Recovery was determined as the percentage change between the flies with the *mid-RNAi* condition (red column) and flies with a heterozygous mutant allele in the background of the *mid-RNAi* condition (blue column). The data sets represented in the bar graph were statistically analyzed using tests as described in detail in section 4.9 of the methods.

Allelic Modifier Studies Place *mid* Genetically within the InR/Akt Signaling Pathway

We undertook allelic genetic modifier studies by placing *mid-RNAi* flies within either heterozygous null mutant alleles and/or transgenic RNAi lines available for genes known to function within the InR/Akt genetic pathway including *dInR, chico, dPI3K, dPTEN, dPDK1, dAkt, dTOR, and Thor*. The *Thor* gene encodes the 4E-BP protein. We also assayed a different mutant allele of *dFOXO, dFOXO*$^{\Delta 94}$. Instead of counting all of the bristles of the compound eye, we counted bristles generated in the dorsal half of the eye since these numbers provided more accurate bristle counts of montaged images obtained from the light compound microscope. All heterozygous mutant alleles and RNAi lines of the InR pathway exhibited normal bristle numbers compared to WT flies (data not shown) and were each independently crossed to *mid-RNAi* flies to carry out the modifier screen. With the exception of *dPDK1* and *Thor*, every mutant allele or transgenic RNAi line of each gene placed in the *mid-RNAi* background significantly suppressed the *mid* mutant phenotype (Table 5).

The most effective suppressors of the *mid-RNAi* phenotype recovered a majority of IOBs and exhibited normal cell morphology, especially within the peripheral region of the eye (Figure 8). Statistically significant suppressors placed in the *UAS-mid-RNAi/+;GMR-Gal4/+* background included *dFOXO*$^{\Delta 94}$, *TRiP-dILP6, TRiP-PI3K*, and *TRiP-PTEN* where compound eye bristles were recovered by approximately 46-59% (Figure 9) (Table 5). The TRiP designation indicates an RNAi transgenic line (Ni et al.,

2009). The *TRiP-dTOR, TRiP-dInR and TRiP-dILP5* compound eyes exhibited a moderate recovery of bristles by 23%, 28%, and 39%, respectively (Figure 9) (Table 5). Less statistically significant suppressors included *TRiP-dILP2*, *TRiP-Chico*, and *TRiP-dAkt* where bristles still were recovered by ~23-66% (Figure 9) (Table 5).

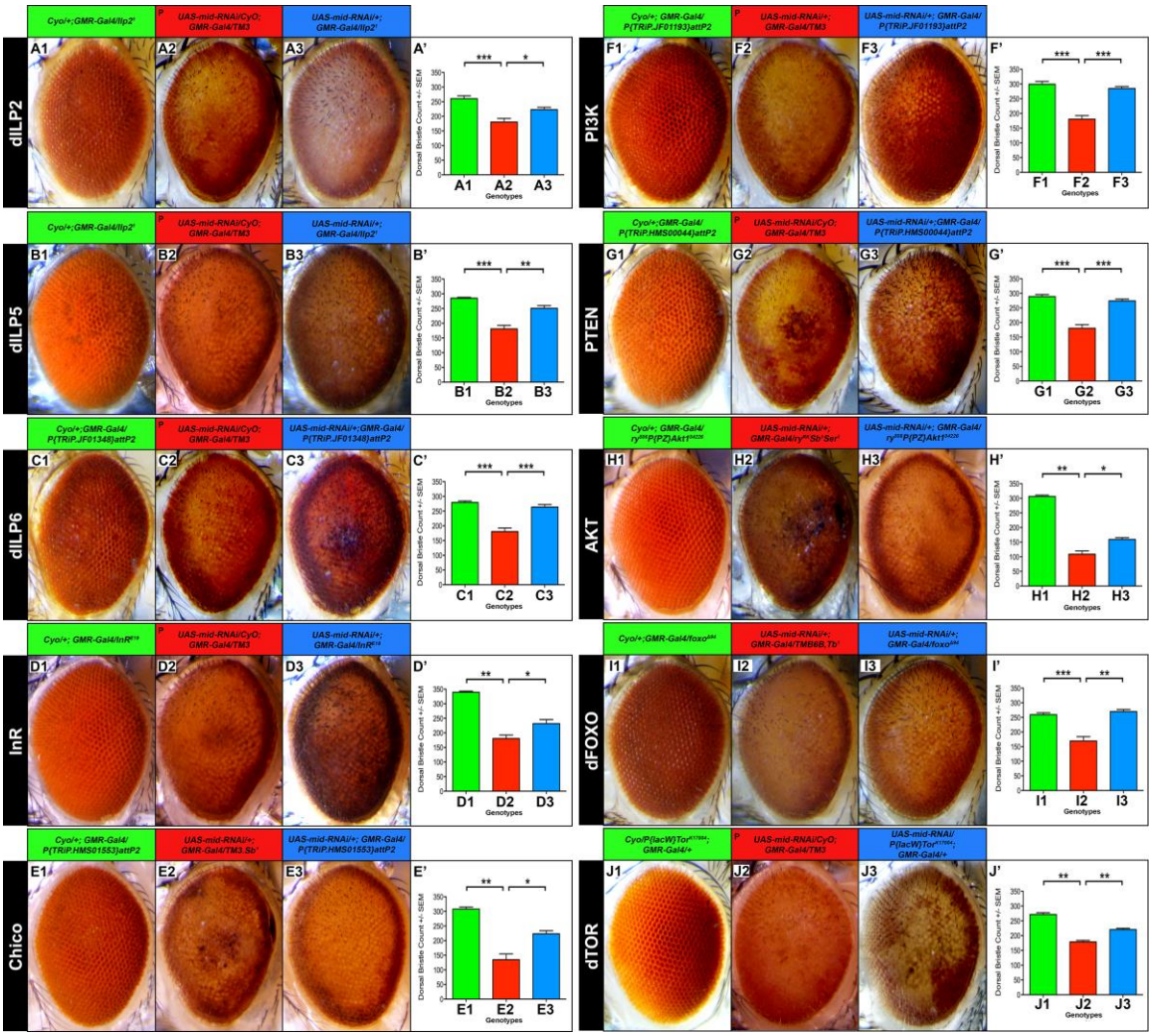

Figure 9. An allelic modifier screen indicates that mid antagonizes most members of the InR signaling pathway. Each horizontal series of panels consists of three images of specific F1 genotypes of the compound eyes of one-day old female progeny generated from the parental cross of *mid-RNAi* flies with a mutant allele or RNAi line available for the allele (designated by *TRiP*) of the InR pathway. These images are followed by a bar graph represented with a primed alphabetical letter. The bar graph summarizes the mean bristle numbers +/- the SEM of each genotype highlighted by green, red, and blue colors that correspond with the coloring of the three matching subpanel titles. The green-labeled genotype represents an F1 progeny heterozygous for both the mutant allele and the GMR-Gal4 driver line which provides a WT phenotype of bristle numbers that are nearly equivalent to those of Oregon-R flies (Das et al., 2013). The red-labeled genotype represents an F1 progeny designated as a *mid-RNAi* condition except where there is a "P". The "P" label indicates that an internal F1 *mid-RNAi* genotype was not generated from the cross and the genotype represents a parental *mid-RNAi* compound eye (*UAS-mid-RNAi/CyO;GMR-Gal4/TM3*). The blue-labeled genotype represents an F1 progeny that places a heterozygous mutant allele or *UAS-RNAi-TRiP* line of an InR pathway member in a *mid-RNAi* background to assay for enhancement or suppression of the *mid-*

RNAi phenotype. Statistical comparisons among designated genotypes are represented by brackets where all comparisons are statistically significant and represented by one, two, or three asterisks. For reviewing the *p*-values represented by the asterisks refer to Table 3. The data sets represented in the bar graph were statistically analyzed using several tests as described in detail in section 4.9 of the methods. The genetic data suggest that *mid* antagonizes most members of the InR receptor pathway. Based upon the broad range of suppression, *mid* appears to genetically antagonize specific alleles in a dosage-dependent manner.

Table 5

Data comparisons from an allelic modifier screen assaying members of the InR/Akt signaling pathway

dILP2	UAS-mid-RNAi/+; TM3/Ilp2[1]	CyO/+;TM3/Ilp2[1]	CyO/+; GMR-Gal4/Ilp2[1]	P UAS-mid-RNAi/CyO; GMR-Gal4/TM3	UAS-mid-RNAi/+; GMR-Gal4/Ilp2[1]	% Recovery	*p*-value
	307±5	272±11	260±10	181±12	223±8	23%	*p*=0.0029
dILP5	UAS-mid-RNAi/+;TM3/ P{TRiP.JF01347}attP2	CyO/+;TM3/ P{TRiP.JF01347}attP2	CyO/+;GMR-Gal4/ P{TRiP.JF01347}attP2	P UAS-mid-RNAi/CyO; GMR-Gal4/TM3	UAS-mid-RNAi/+; GMR-Gal4/ P{TRiP.JF01347}attP2	% Recovery	*p*-value
	314±7	288±9	285±3	181±12	251±9	39%	*p*=0.0002
dILP6	UAS-mid-RNAi/+;TM3/ P{TRiP.JF01348}attP2	CyO/+;TM3/ P{TRiP.JF01348}attP2	CyO/+;GMR-Gal4/ P{TRiP.JF01348}attP2	P UAS-mid-RNAi/CyO; GMR-Gal4/TM3	UAS-mid-RNAi/+; GMR-Gal4/ P{TRiP.JF01348}attP2	% Recovery	*p*-value
	346±7	304±9	279±5	181±12	263±8	46%	*p*<0.0001
InR	UAS-mid-RNAi/+; GMR-Gal4/InR^{E19}	CyO/+; TM3/InR^{E19}	CyO/+; GMR-Gal4/InR^{E19}	P UAS-mid-RNAi/CyO; GMR-Gal4/TM3	UAS-mid-RNAi/+; GMR-Gal4/InR^{E19}	% Recovery	*p*-value
	322±8	301±5	339±4	181±12	232±14	28%	*p*=0.0091
Chico	UAS-mid-RNAi/+;TM3,Sb[1]/ P{TRiP.HMS01553}attP2	CyO/+;TM3/ P{TRiP.HMS01553}attP2	CyO/+;GMR-Gal4/ P{TRiP.HMS01553}attP2	UAS-mid-RNAi/+; GMR-Gal4/TM3,Sb[1]	UAS-mid-RNAi/+; GMR-Gal4/ P{TRiP.HMS01553}attP2	% Recovery	*p*-value
	295±6	320±7	308±7	135±20	223±11	66%	*p*=0.0058
PI3K	UAS-mid-RNAi/+;TM3/ P{TRiP.JF01193}attP2	CyO/+;TM3/ P{TRiP.JF01193}attP2	CyO/+;GMR-Gal4/ P{TRiP.JF01193}attP2	P UAS-mid-RNAi/CyO; GMR-Gal4/TM3	UAS-mid-RNAi/+; GMR-Gal4/ P{TRiP.JF01193}attP2	% Recovery	*p*-value
	316±6	299±9	285±4	181±12	231±7	28%	*p*<0.0001
PTEN	UAS-mid-RNAi/+;TM3/ P{TRiP.HMS00044}attP2	CyO/+;TM3/ P{TRiP.HMS00044}attP2	CyO/+;GMR-Gal4/ P{TRiP.HMS00044}attP2	P UAS-mid-RNAi/CyO; GMR-Gal4/TM3	UAS-mid-RNAi/+; GMR-Gal4/ P{TRiP.HMS00044}attP2	% Recovery	*p*-value
	319±7	310±6	289±7	181±12	274±6	52%	*p*<0.0001
AKT	UAS-mid-RNAi/+;TM3/ ry^{506}P{PZ}Akt1^{04226}	CyO/+;TM3/ ry^{506}P{PZ}Akt1^{04226}	CyO/+;GMR-Gal4/ ry^{506}P{PZ}Akt1^{04226}	UAS-mid-RNAi/+; GMR-Gal4/TM3	UAS-mid-RNAi/+; GMR-Gal4/ ry^{506}P{PZ}Akt1^{04226}	% Recovery	*p*-value
	348±6	312±8	306±5	109±11	159±6	47%	*p*=0.0172
dFOXO	UAS-mid-RNAi/+;TM3/ dFOXO$^{\Delta 94}$	CyO/+; TM3/dFOXO$^{\Delta 94}$	CyO/+; GMR-Gal4/dFOXO$^{\Delta 94}$	UAS-mid-RNAi/+; GMR-Gal4/TM6B.Tb[1]	UAS-mid-RNAi/+; GMR-Gal4/dFOXO$^{\Delta 94}$	% Recovery	*p*-value
	351±6	318±9	259±6	170±14	270±7	59%	*p*=0.0002
dTOR	UAS-mid-RNAi/+;TM3/ P{TRiP.GL00156}attP2	CyO/+;TM3/ P{TRiP.GL00156}attP2	CyO/+;GMR-Gal4/ P{TRiP.GL00156}attP2	UAS-mid-RNAi/+; GMR-Gal4/TM3	UAS-mid-RNAi/+; GMR-Gal4/ P{TRiP.GL00156}attP2	% Recovery	*p*-value
	323±10	312±8	272±6	179±5	220±5	23%	*p*=0.0002

Note. Each column represents a specific genotype and the mean dorsal IOB count +/- SEM. The first two uncolored columns are additional F1 progeny recovered in the genetic modifier screens which do not carry the *GMR-Gal4* driver line. The green, red, and blue labeled columns correspond to the similarly labeled genotypes shown in Figure 3. Recovery was determined as the percentage change between the flies with the *mid-RNAi* condition (red column) and flies with a heterozygous mutant allele in the background of the *mid-RNAi* condition (blue column). The data sets represented in the bar graph were statistically analyzed using tests as described in detail in section 4.9 of the methods.

Allelic Modifier Studies Place *mid* Genetically within the JNK Signaling Pathway

Similarly, we carried out an additional allelic modifier study by placing *mid-RNAi* flies within either heterozygous null mutant alleles or RNAi lines available for genes known to function within the JNK signaling pathway. We found that the compound eyes of flies with *TRiP-hep, TRiP-cka, TRiP-bsk, and TRiP-fos* placed in the *mid-RNAi* background exhibited a significantly suppressed *mid-RNAi* phenotype, where bristles were recovered by 26-46% (Figure 10) (Table 6). Less significantly, the *mid-RNAi* mutant phenotype was suppressed with *TRiP-slpr* and *TRiP-jun* with a recovery of ~16% and ~41% bristles, respectively (Figure 10) (Table 6). The *UAS-mid-RNAi/+;GMR-Gal4/puc*^{DN} compound eyes also showed a suppressed *mid-RNAi* phenotype where bristles were recovered by ~27% (Figure 10G) (Table 6). Based upon these results, we propose that *mid* functions downstream of *bsk* within the JNK signaling pathway to antagonize InR/Akt signaling by relieving a negative feedback inhibition loop mediated by Puc to block Bsk activity (Figure 10H). In addition, *mid* antagonizes the JNK pathway at the level of *hep* and *cka* (Figure 10B).

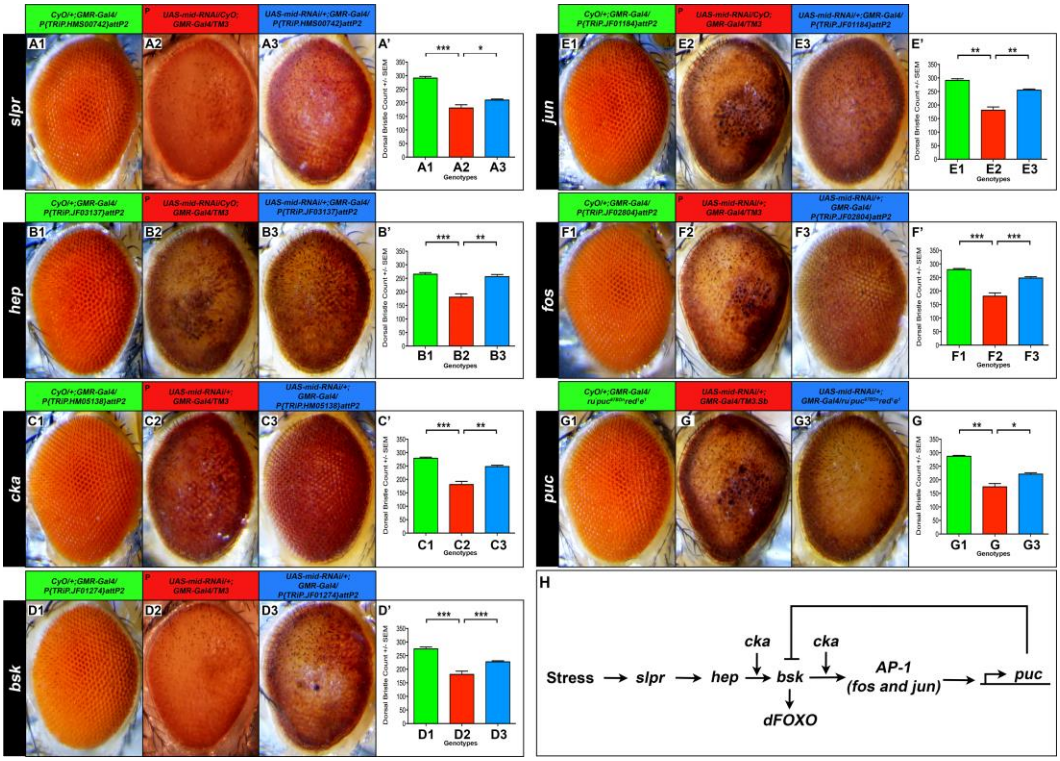

Figure 10. An allelic modifier screen shows that mid antagonizes specific JNK pathway members. Each horizontal series of panels consists of three images of specific F1 genotypes of the compound eyes of one-day old female progeny generated from the parental cross of *mid-RNAi* flies with a mutant allele or RNAi line available for the allele (designated by *TRiP*) of the JNK pathway. These images are followed by a bar graph represented with a primed alphabetical letter that summarizes the mean bristle numbers +/- the SEM of each genotype highlighted by the green, red, and blue colors shown on the first three subpanel titles corresponding with the colored bars of the graph. The green-labeled genotype represents an F1 progeny heterozygous for both the mutant allele and the *GMR-Gal4* driver line which provides a WT phenotype of bristle numbers that are nearly equivalent to those of OR flies (Das et al., 2013). The red-labeled genotype represents an F1 progeny designated as a *mid-RNAi* condition except where there is a "P". The "P" label indicates that an internal F1 *mid-RNAi* genotype was not generated from the cross and the genotype represents a parental *mid-RNAi* compound eye (*UAS-mid-RNAi/CyO;GMR-Gal4/TM3*). The blue-labeled genotype represents an F1 progeny in which a heterozygous mutant allele or *UAS-RNAi-TRiP* line of a JNK pathway member is placed within a *mid-RNAi* background to assay for enhancement or suppression of the *mid-RNAi* phenotype. Statistical comparisons among designated genotypes are represented by brackets where all comparisons are statistically significant and represented by one, two, or three asterisks. For reviewing the *p*-values represented by the asterisks refer to Table 4. The data sets represented in the bar graph were statistically analyzed using several tests as described in detail in section 4.9 of the methods. The genetic data suggest that *mid* antagonizes seven members of the JNK pathway in a dosage-dependent manner. (H) The schematic represents the genetic hierarchy of the JNK signaling pathway.

Table 6

Data comparisons from an allelic modifier screen assaying members of the JNK signaling pathway

slpr	*UAS-mid-RNAi/+;TM3/ P{TRiP.HMS00742}attP2*	*CyO/+;TM3/ P{TRiP.HMS00742}attP2*	*CyO/+;GMR-Gal4/ P{TRiP.HMS00742}attP2*	*P UAS-mid-RNAi/CyO; GMR-Gal4/TM3*	*UAS-mid-RNAi/+; GMR-Gal4/ P{TRiP.HMS00742}attP2*	**% Recovery**	***p*-value**
	296±6	**295±5**	**291±6**	**181±12**	**210±4**	**16%**	***p*=0.0014**
hep	*UAS-mid-RNAi/+;TM3/ P{TRiP.JF03137}attP2*	*CyO/+;TM3/ P{TRiP.JF03137}attP2*	*CyO/+;GMR-Gal4/ P{TRiP.JF03137}attP2*	*P UAS-mid-RNAi/CyO; GMR-Gal4/TM3*	*UAS-mid-RNAi/+; GMR-Gal4/ P{TRiP.JF03137}attP2*	**% Recovery**	***p*-value**
	295±5	**263±9**	**265±6**	**181±12**	**256±8**	**42%**	***p*<0.0001**
cka	*UAS-mid-RNAi/+;TM3/ P{TRiP.HM05138}attP2*	*CyO/+;TM3/ P{TRiP.HM05138}attP2*	*CyO/+;GMR-Gal4/ P{TRiP.HM05138}attP2*	*P UAS-mid-RNAi/+; GMR-Gal4/TM3*	*UAS-mid-RNAi/+; GMR-Gal4/ P{TRiP.HM05138}attP2*	**% Recovery**	***p*-value**
	330±7	**305±6**	**279±4**	**181±12**	**248±5**	**37%**	***p*=0.0002**
bsk	*UAS-mid-RNAi/+;TM3/ P{TRiP.JF01274}attP2*	*CyO/+;TM3/ P{TRiP.JF01274}attP2*	*CyO/+;GMR-Gal4/ P{TRiP.JF01274}attP2*	*P UAS-mid-RNAi/CyO; GMR-Gal4/TM3*	*UAS-mid-RNAi/+; GMR-Gal4/ P{TRiP.JF01274}attP2*	**% Recovery**	***p*-value**
	325±6	**307±3**	**275±7**	**181±12**	**227±4**	**26%**	***p*<0.0001**
jun	*UAS-mid-RNAi/+;TM3/ P{TRiP.JF01184}attP2*	*CyO/+;TM3/ P{TRiP.JF01184}attP2*	*CyO/+;GMR-Gal4/ P{TRiP.JF01184}attP2*	*P UAS-mid-RNAi/CyO; GMR-Gal4/TM3*	*UAS-mid-RNAi/+; GMR-Gal4/ P{TRiP.JF01184}attP2*	**% Recovery**	***p*-value**
	344±6	**295±7**	**291±6**	**181±12**	**255±4**	**41%**	***p*=0.0002**
fos	*UAS-mid-RNAi/+;TM3/ P{TRiP.JF02804}attP2*	*CyO/+;TM3/ P{TRiP.JF02804}attP2*	*CyO/+;GMR-Gal4/ P{TRiP.JF02804}attP2*	*P UAS-mid-RNAi/+; GMR-Gal4/TM3*	*UAS-mid-RNAi/+; GMR-Gal4/ P{TRiP.JF02804}attP2*	**% Recovery**	***p*-value**
	337±7	**316±4**	**294±5**	**181±12**	**263±9**	**46%**	***p*<0.0001**
puc	*UAS-mid-RNAi/+;TM3/ $ru^{1}puc^{67BDn}red^{1}e^{1}$*	*CyO/+;TM3/ $ru^{1}puc^{67BDn}red^{1}e^{1}$*	*CyO/+;GMR-Gal4/ $ru^{1}puc^{67BDn}red^{1}e^{1}$*	*UAS-mid-RNAi/+; GMR-Gal4/TM3.Sb*	*UAS-mid-RNAi/+; GMR-Gal4/ $ru^{1}puc^{67BDn}red^{1}e^{1}$*	**% Recovery**	***p*-value**
	350±3	**287±3**	**320±5**	**174±12**	**221±5**	**27%**	***p*=0.0028**

Note. Each column represents a specific genotype and the mean dorsal IOB +/- SEM count. The first two uncolored columns are additional F1 progeny recovered in the genetic modifier screens which do not carry the *GMR-Gal4* driver line. The green, red, and blue labeled columns correspond to the similarly labeled genotypes shown in Figure 4. Recovery was determined as the percentage change between the flies with the *mid-RNAi* condition (red column) and flies with a heterozygous mutant allele in the background of the *mid-RNAi* condition (blue column). The data sets represented in the bar graph were statistically analyzed using tests as described in detail in section 4.9 of the methods.

Mid Exhibits a Nuclear and Cytoplasmic Distribution

Based upon the broad scope of the genetic data, we addressed the possibility that Mid may interact directly or indirectly within N, InR/Akt, and/or JNK signaling pathway members located within the cytoplasm and/or nucleus to regulate neuronal cell fate specification and survival. Moreover, from previous immunofluorescent antibody labeling studies with specific cytoplasmic and nuclear markers, we detected Mid and its paralog H15 expressed within both the cytoplasm and nucleus of wild-type (WT) Oregon-R (OR) eye imaginal discs of third-instar (3^oL) larvae (data not shown). To biochemically confirm that Mid and H15 exhibits a cytoplasmic and nuclear distribution, we undertook Western analyses of nuclear and cytoplasmic extracts isolated from OR and *UAS-mid-RNAi/CyO;GMR-Gal4/TM3* 3^oL whole tissue homogenates (Figure 11). The western blot shows a Mid-specific band migrating at approximately 72 kDa in both the cytoplasm and nucleus of OR and *mid*-RNAi (Figure 11). However, the Mid distribution in *mid*-RNAi appears to be slightly more cytoplasmic compared to that of OR. Mid also displayed a doublet band in the nuclear fraction, perhaps suggesting that Mid may have been phosphorylated. The Mid band is also not a clean solid band but instead had a smear effect similar to the running of DNA. Curiously, H15 was found to be completely within the cytoplasmic fraction as well as running at approximately 36 kDa, half of the expected weight of 72 kDa (Figure 11). We confirmed clean fractionation by observing Lamin C within the nuclear fractions and β-tubulin within the cytoplasmic fractions.

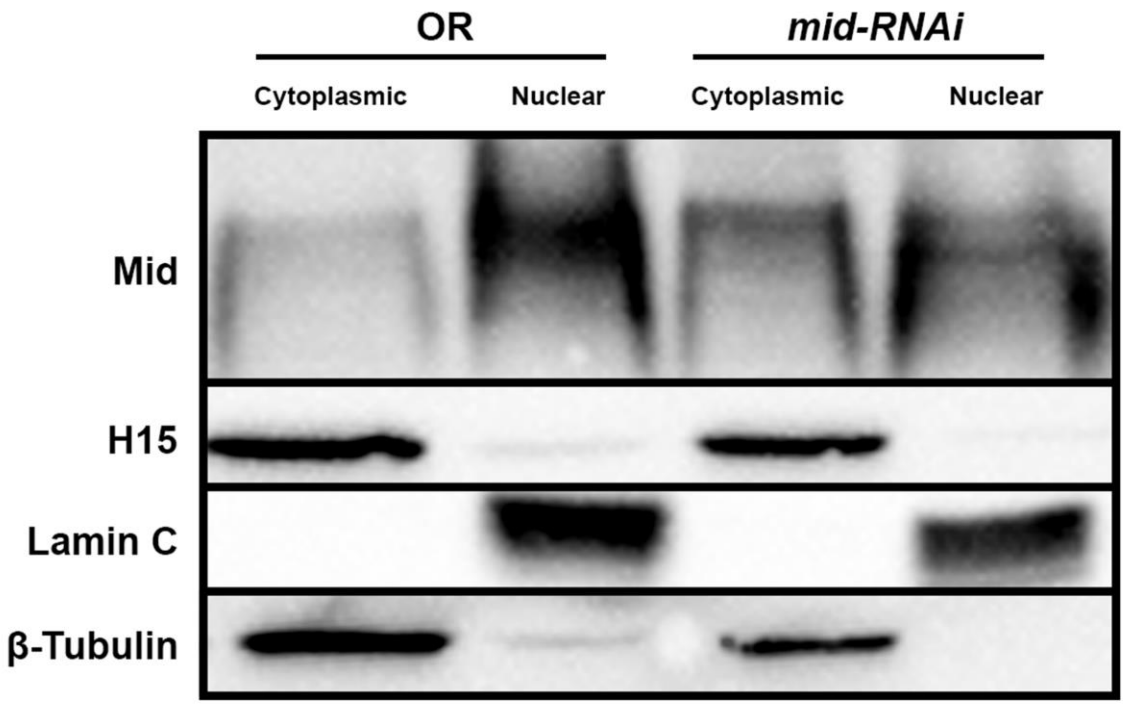

Figure 11. Mid is detected in both the cytoplasm and nucleus of WT 3^{o}L tissues. Western blot analysis indicates that Mid is expressed within cytoplasmic and nuclear fractions isolated from 3^{o}L whole tissue homogenates. Mid expression is found to be more cytoplasmic and less nuclear in *mid*-RNAi conditions compared to OR. H15 is entirely cytoplasmic and not found within the nuclear fraction. Lamin C and β–Tubulin were used as loading controls for the nuclear and cytoplasmic fraction, respectively.

A Low Level of Paraquat-induced Oxidative Stress Suppresses the *mid*-RNAi Mutant Phenotype by Partially Recovering IOBs

Since the JNK pathway reacts to oxidative stress by neutralizing reactive oxygen species (ROS) (McCubrey, LaHair, & Franklin, 2006) and Mid genetically antagonizes several JNK pathway members, we determined whether oxidative stress affects the development of IOBs in WT and *mid-RNAi* mutant flies. Three-day old 3^{o}L were fed 0.5% yeast paste alone or 0.5% yeast paste containing increasing doses of paraquat (1, 5, 10, 20, and 30 mM) until eclosion approximately 5 days later (Figure 12A). Paraquat increases ROS and is a neurotoxic reagent (Mollace et al., 2003). We found that larvae fed with 1 mM paraquat generated viable, one-day old adult OR and *mid-RNAi* mutant flies (Figure 12A). While 1 mM paraquat-treated OR flies developed normally they exhibited lower numbers of IOBs compared to untreated OR flies (Figure 12A). Conversely, the eyes of 1 mM paraquat-treated *mid-RNAi* flies exhibited significantly higher numbers of bristles than untreated *mid-RNAi* flies (Figure 12A). Increased doses of paraquat at 5, 10, and 20 mM gradually restored the IOB bristle count of OR and *mid-RNAi* mutant flies to that detected at 0 mM paraquat (Figure 12A). Treatment with a 30 mM dose of paraquat resulted in poor brain development in some larvae as well as a headless phenotype in surviving adult *mid-RNAi* flies (data not shown).

We next determined whether inducing metabolic stress via a starvation paradigm affected the development of IOBs in one-day old female WT and *mid-RNAi* flies. Following a starvation period of 24 hours during late 3^{o}L stages, both WT and *mid-RNAi* flies exhibited a concomitant decrease in IOBs (Figure 12B) and eye size (data not shown). Such a result suggests that *mid* is genetically active within the Akt and JNK

signaling pathways in association with oxidative stress to regulate SOP cell fate specification and bristle formation.

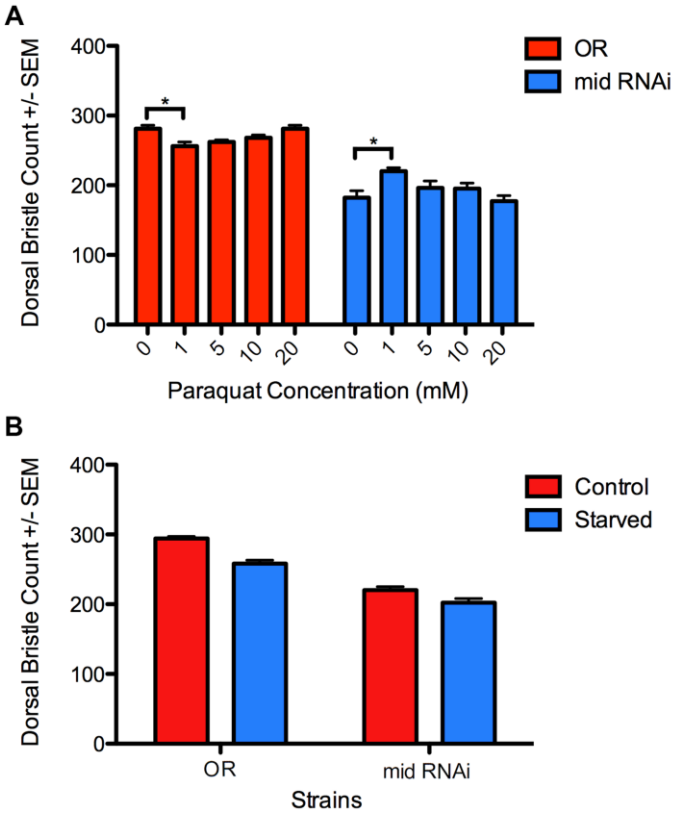

Figure 12. A low level of paraquat-induced oxidative stress suppress the *mid*-RNAi mutant IOB phenotype while metabolic stress has no effect on the mid mutant phenotype. Dorsal interommatidial bristles were counted from OR and *mid-RNAi* flies treated with increasing dosages of paraquat (0mM, 1mM, 5mM, 10mM, and 20mM) to induce oxidative stress. (A) While a 1 mM dose of paraquat results in a 9% loss of bristles compared to untreated (0 mM paraquat) WT flies ($p^* = 0.0018$), *mid-RNAi* flies fed 1 mM paraquat exhibit a 21% recovery of bristles compared to untreated *mid-RNAi* flies ($p^* = 0.0237$). Increasing doses of paraquat gradually recover bristle counts to the baseline levels detected at 0 mM paraquat (untreated flies) in both WT and *mid-RNAi* strains. (B) Induction of metabolic stress through starvation results in a similar loss of bristles in both OR (12% loss) and *mid-RNAi* (8% loss) flies. We scored 30 eyes for IOB counts for all control and experimental groups. The error bars denote the mean bristle count +/- SEM. The *p* values are assessed by one-factor ANOVA and Tukey's Honest Significant Difference (HSD).

CHAPTER IV

DISCUSSION

Mid Antagonistically Regulates dFOXO

Through our allelic modifier screen to enhance or suppress a *mid*-RNAi mutant phenotype with members of the InR and JNK signaling pathway, we present evidence of *mid* antagonism with members of both signaling pathways and most significantly, *dFOXO*. These results suggest that Mid antagonistically interacts with the InR and JNK pathways upstream of dFOXO.

We propose a model in which Mid complexes with the co-repressors of Su(H), Gro, H, and CtBP, to compete with the co-activator complex of Su(H), dFOXO, Mam, and N_{ICD} for binding affinity to Su(H) (Figure 13). Based on our model, Mid prevents dFOXO from removing the co-repressors of Su(H) in the absence of the N_{ICD}. Thus, within wild-type pre-SOP cells, Su(H) inhibits *E(spl)* and drives proneural SOP cell fate adoption. Under *mid*-RNAi conditions, however, the weakened co-repressor complex can no longer prevent dFOXO from ejecting the co-repressors and thereby activates Su(H) without N_{ICD}. Activated Su(H) drives expression of *E(spl)* which promotes the adoption of the epithelial cell fate. It is possible that specification of potential proneural SOP cells into epithelial cells yields the *mid*-RNAi mutant eye phenotype. Upon introduction of a *dFOXO* loss-of-function mutant allele in the background of the *mid*-RNAi phenotype, we detected a nearly complete recovery of SOP neuronal cell fates, suggesting that a stoichiometric balance between Mid and dFOXO is required to regulate Su(H) activation.

Previous evidence supports our model by placing *mid* genetically within the Notch/Delta signaling pathway downstream of *N* but upstream of *E(spl)* in the genetic

hierarchy (Das et al., 2013). Further, Mid has previously been suggested to directly bind with Gro via Mid's Engrailed homology-1 domain to regulate the segment polarity gene *wingless* (Formaz-Preston, Ryu, Svendsen, & Brook, 2011). Mid interaction with Gro is also conserved in mammalian and amphibian systems as well: studies report TBX-20, binds directly with the Gro ortholog, Transducin-like Enhancer of Split (TLE) (Kaltenbrun et al., 2013). Additional evidence has suggested that Foxo1, the mammalian homolog of dFOXO, plays a crucial role in removing the co-repressors of Csl, the mammalian homolog of Su(H), in complex with the Mam/N_{ICD} (Kitamura et al., 2007). The removal of the Csl co-repressors increases expression of Hes1, the mammalian homolog of E(spl), within *in vitro* mouse cell cultures (Kitamura et al., 2007). Past studies have indicated an intrinsic link between the Notch, InR, and JNK signaling pathways in regard to the development of a multitude of tissues (Dutriaux, Godart, Brachet, & Silber, 2013; Hsu & Drummond-Barbosa, 2011; Zecchini, Brennan, & Martinez-Arias, 1999). Most recently, the InR and Notch signaling pathways were reported to regulate the bristle formation of the peripheral nervous system (Dutriaux et al., 2013). Taken together, the evidence appears to support the model that Mid is involved in a co-repressor/co-activator relationship with dFOXO to regulate Su(H) at the *E(spl)* enhancer region.

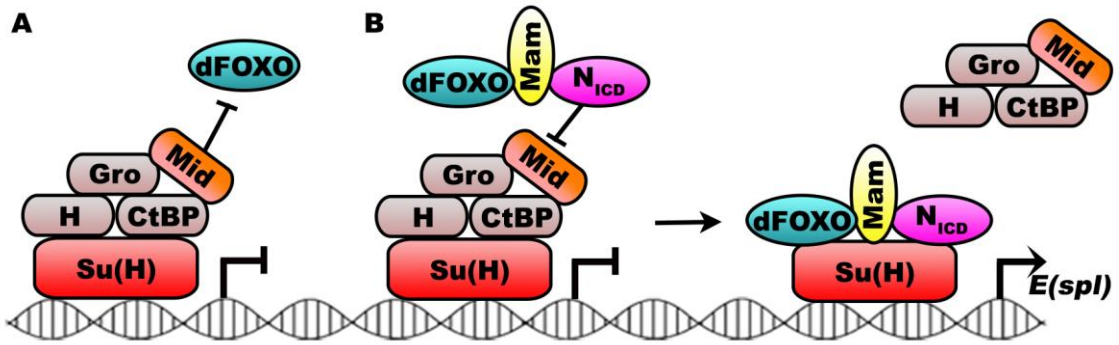

Figure 13. A model depicting the hypothetical mechanism by which Mid and dFOXO interact to regulate neuronal SOP cell fates. Mid functions to preserve Gro-H-CtBP co-repression of Su(H) in the absence of N_{ICD}. (A) Without the nuclear localization of N_{ICD} to form a complex with dFOXO, Mid prevents dFOXO from removing corepressors of Su(H) and leads to the adoption of the SOP cell fate. (B) Nuclear translocation of N_{ICD} to complex with dFOXO bypasses Mid inhibition of dFOXO and allows dFOXO to exchange Su(H) corepressors Gro-H-CtBP for co-activator Mastermind. This results in expression of *E(spl)* and the adoption of the epithelial cell fate.

Mid Exhibits Bifunctional Regulation of the InR and JNK pathways

From our proposed model, we expect that in the *mid*-RNAi background, decreased dFOXO activity via disruption of the JNK pathway results in the Mid-co-repressor complex keeping Su(H) in a co-repressive state and as a result, more cells adopt the SOP cell fate to create a suppression of the *mid*-RNAi phenotype. Likewise, upregulating dFOXO via the InR pathway should lead to an increased conversion of Su(H) into a co-activator and enhance the *mid*-RNAi phenotype. However, our results did not agree with this prediction. In contrast, disruption of many InR alleles placed in the *mid*-RNAi background suppresses the *mid*-RNAi phenotype and recovers bristles. Curiously, allelic modifier candidates that were antagonistic to the InR and JNK pathways such as *PTEN* and *puckered*, respectively, did not enhance the *mid*-RNAi phenotype. Decreased PTEN and Puckered both suppressed the *mid*-RNAi phenotype.

In the InR pathway, PTEN represses PI3K by converting the protein back into PI2K and inhibits AKT signaling. Thus, we expected reduced PTEN to enhance the *mid*-

RNAi phenotype. Oddly, we found that Mid antagonistically regulated AKT and PTEN signaling. PTEN, a tumor suppressor gene, has been shown to promote apoptosis when overexpressed in the *Drosophila* eye (Huang et al., 1999). Further, as an inhibitor of cell growth, reduced PTEN expression has been shown to induce cell proliferation (Huang et al., 1999). The increased levels of apoptosis seen in Das et al. (2013) in the *mid*-RNAi eye may have resulted from increased *PTEN* expression. When we knocked down both *PTEN* and *mid* expression together we may have returned apoptotic-signaling levels back to normal and recovered bristles.

The results with *puckered* also suggest that there may be cross-talk with other pathways involving the JNK pathway. The JNK pathway, for example, is involved in compensatory proliferation and is expressed in cells near apoptotic cells in response to cellular injury. This proliferative pathway utilizes Decapentaplegic and Wingless signals secreted from the apoptotic cells as well as pro-apoptotic genes *reaper* and *hid* (Ryoo, Gorenc, & Steller, 2004). We may have activated a cellular proliferative aspect of JNK instead of the apoptotic pathway, or both in competition, when we reduced *puckered* expression in the *mid*-RNAi background. Apoptotic cells releasing Reaper and Hid may initiate proliferative pathways in nearby non-apoptotic cells as compensation. These results with PTEN and Puckered suggest that Mid may serve a bifunctional role in regulating the InR and JNK signaling pathways.

The *mid*-RNAi Phenotype is Responsive to Oxidative Stress

We attempted to determine the effects of metabolic and oxidative stress using a starvation and paraquat exposure paradigm, respectively. The results showed that induction of metabolic stress through starvation did not have a significant effect on the

mid-RNAi phenotype compared to wild-type flies. Both starved strains resulted in a smaller bristle count but the flies were smaller in general as well as specifically in the ommatidium. This decrease in size as a result of starvation has been reported previously, suggesting that the effect of starvation is primarily due to elements of the InR pathway instead of an interaction between *mid* and the InR pathway under starvation (Tu & Tatar, 2003). However, the starvation paradigm is only one aspect of AKT signal regulation.

As reported, we found a significantly different response toward oxidative stress between OR and *mid*-RNAi strains exposed to paraquat at 3^{o}L. At 1 mM paraquat, we found that OR strains had a significant decrease in ommatidial bristles while *mid*-RNAi strains demonstrated a significant increase in ommatidial bristles. As the dosage of paraquat increases, the ommatidial bristles gradually return back to match the results of the 0mM control. At low doses, JNK may be activated under *mid*-RNAi conditions to neutralize reactive oxygen species and recover bristles. Oxidative stress activates the JNK and increases dFOXO activity and is effectively an indirect gain-of-function dFOXO assay. This suggests that *mid* may play a pro-apoptotic role under low oxidative stress. At high levels of stress, there may be an averaging of effect through cross talk with various other pathways, in addition to the JNK, which leads to the gradual restoration of the *mid*-RNAi phenotype.

Our findings deviate from the model hypothesized in Calnan and Brunet (2008) in which JNK invokes differential responses based on the amount of stress within the cells. In their model, low levels of stress initiate a pro-survival response to resist stress while high levels of stress active an apoptotic response by JNK. Here, we find the opposite is true with low levels of stress inducing bristle loss in wild-type flies and high levels of

stress resulting in cellular resilience. It is possible that our results deviate from the Calnan and Brunet model due to flies refusing to ingest the food containing higher doses of paraquat. The flies may sense a disturbance in the food and refuse to eat it as 3^{o}L. Thus, the flies were never truly exposed to the high levels of paraquat and subsequently reflected bristle counts similar to that of the 0 mM control. If such an event occurred, it is possible that Calnan and Brunet's model still holds where high dosages of oxidative stress through paraquat causes JNK to induce apoptosis instead of conferring stress resistance. We would predict that after an initial increase of bristles in the *mid*-RNAi flies at low doses, there would be a gradual decrease in bristles as the dosages increased. Overall, our results show a differential response to low levels of paraquat between OR and *mid*-RNAi flies which supports *mid* interaction through the JNK as a pro-apoptotic element.

Mid and H15 are Detected in the Cytoplasm and Nucleus

Through Western blot analysis, we detected Mid and H15 within the cytoplasmic fraction, a phenomenon not yet shown in literature but observed via immunofluorescence of the T-box gene Tbx-20 in fibroblast cells (Stennard et al., 2003) and Tbx-5 in chicken hearts (Bimber, Dettman, & Simon, 2007). After testing H15 protein levels, we found that H15 was almost exclusively cytoplasmic and H15 levels remained constant in the *mid*-RNAi strain compared to OR. This result, in addition to the significant decrease in size, is very curious. Although a paralog to Mid and sharing 89% identity, H15's function has been less characterized and often only in conjunction with Mid (Buescher et al., 2006; Leal et al., 2009; Miskolczi-MaCallum et al., 2005; Qian et al., 2005; Svendsen, Formaz-Preston, Leal, & Brook, 2009). In the *mid*-RNAi flies, levels of Mid

were found to be increased in the cytoplasmic fraction and decreased within the nuclear fraction compared to OR. It is possible that the *mid*-RNAi effect caused a cytoplasmic relocalization to effect upstream targets of dFOXO such as the InR receptor or Bsk. Surprisingly, the levels of Mid loss within the *mid*-RNAi strain were much higher than hypothesized considering that the *mid*-RNAi effect was thought to be localized exclusively to the eye using GMR-Gal4. This suggests that the GMR-Gal4 may have off-target effects and causes a decrease of *mid* expression in other tissue types as described in previous studies (Li, Li, Zheng, Zhang, & Xue, 2012).

CHAPTER V

FUTURE DIRECTIONS

The central aim of this thesis is to elucidate *mid*'s transcriptional network and to specifically uncover *mid*'s interaction with *dFOXO,* a vital component of several developmental and physiological pathways, within the model organism *Drosophila melanogaster*. These studies have taken steps towards achieving the aims but must be further clarified in the future in order to achieve a full understanding of *mid*'s gene regulatory network.

Test the Proposed Model

While these studies have led to the formation of a proposed model in which Mid antagonizes dFOXO directly as a co-repressor of Su(H), we must test the model. First, we can examine Mid binding affinity to Su(H) and Gro by co-immunoprecipition (co-IP) to demonstrate that Mid is a factor within the Su(H) co-repressive complex. This experiment is critical in determining the exact mechanism in which Mid antagonizes dFOXO. The current model, in conjunction with recent literature, hypothesizes that Mid directly binds to the co-repressor complex to inhibit dFOXO's ability to remove the co-repressors from Su(H) but is still unconfirmed (Kaltenbrun et al., 2013).

In addition to co-IP, probing the differential expression of *E(spl)* between OR and *mid*-RNAi flies would provide further support for our model. In collaboration with Dr. Glenmore Shearer, we can perform this experiment with qRT-PCR to measure the *E(spl)* expression levels. Under our model, *mid*-RNAi flies should express increased of *E(spl)* compared to OR.

Examine Other Metabolic Stressors

In our metabolic stress experiment, we eliminated nutrient intake as a source of stress. In doing so, we effectively inhibited the AKT pathway to alter dFOXO activity. We saw a similar decrease in bristle numbers in both OR and *mid*-RNAi flies but detected that both strains were smaller in overall size (data not shown). The small size confirms that the AKT pathway was, at minimum, altered to limit growth and proliferation. Members within the lab are currently examining the effects of the reciprocal stress, excess nutrients and glucose, on the *mid*-RNAi phenotype by feeding the flies food supplemented with additional fat or sucrose. In these experiments, AKT would experience increased activation to inhibit dFOXO by cytoplasmic sequestration. This may exacerbate the *mid*-RNAi phenotype and lead to a decrease of IOBs. If we detect increased IOB loss, we could further confirm increased cytoplasmic sequestration of dFOXO as well as examine Mid response via western blot analysis of nucleocytoplasmic fractions.

Explore GMR-Gal4 Off Target Effects

Our examination of *mid*-RNAi effects utilizes the UAS/Gal4 binary system developed by Brand and Perrimon (1993) in conjunction with GMR-Gal4, an eye specific promoter. Recent studies have shown that GMR-Gal4 has off target effects in the leg and wings in addition to the eye (Li et al., 2012). Thus, studying the off target effects of *mid*-RNAi may be helpful in elucidating the true interaction between *dFOXO* and *mid*. Fat bodies, for example, release InR-pathway-activating dILP proteins which we found to be antagonized by *mid* genetically. The fat body and salivary gland also sends mitogenic signals to the eye imaginal disc to begin cellular proliferation (Delanoue et al., 2010;

Germinard et al., 2009; Kannan & Fridell, 2013). We can perform immunofluorescence to examine *mid* expression levels in various tissues of the *mid*-RNAi strain. There may be off target effects on the fat body, brain, or salivary glands which, when identified, can allow us to fully understand the implications of *mid*-RNAi expression by GMR-Gal4.

Develop the *mid* Gene Regulatory Network

Currently, we have performed genetic modifier screens utilizing chromosomal deficiencies to identify potential *mid* interacting candidates. In the future, we can perform ChIP-seq using anti-Mid antibody to determine global DNA binding sites for Mid. These binding sites would provide targeted *mid*-interacting candidates to explore further. If our proposed model holds, Mid would be observed at the enhancer region of *E(spl)*. Additionally, we could utilize RNA-seq to look at global differential expression changes resulting from *mid*-RNAi knockdown in various tissues and developmental time points. This, in conjunction with the ChIP-seq binding site data, can extensively refine our target pool outside of the CNS and eye model systems.

REFERENCES

Artavanis-Tsakonas, S., Matsuno, K., & Fortini, M.E. (1995). Notch Signaling. *Science, 268*(5208), 225-232.

Barolo, S., Stone, T., Bang, A.G., & Posakony, J.W. (2002). Default repression and Notch signaling: Hairless acts as an adaptor to recruit the corepressors Groucho and dCtBP to Suppressor of Hairless. *Genes & Development, 16*(15), 1964-1976.

Barolo, S., & Posakony, J.W. (2002). Three habits of highly effective signaling pathways: principles of transcriptional control by developmental cell signaling. *Genes & Development, 16*(10), 1167-1181.

Bimber B, Dettman R.W., & Simon H-G. (2007). Differential regulation of Tbx5 protein expression and sub-cellular localization during heart development. *Developmental Biology, 302*(1), 230-242.

Brand, A.H., & Perrimon, N. (1993). Targeted gene expression as a means of altering cell fates and generating dominant phenotypes. *Development, 118*(2), 401-415.

Brunet, A., Bonni, A., Zigmond, M.J., Lin, M.Z., Juo, P., Hu, L.S., Anderson, M.J., Arden, K.C., Blenis, J., & Greenberg, M.E. (1999). Akt promotes cell survival by phosphorylating and inhibiting a Forkhead transcription factor. *Cell, 96*(3), 857-868.

Buescher, M., Svendsen, P.C., Tio, M., Miskolczi-McCallum, C., Tear, G., Brook, W.J., & Chia, W. (2004). *Drosophila* T box proteins break the symmetry of hedgehog-dependent activation of wingless. *Current Biology, 14*(19), 1694-1702.

Calnan, D.R., & Brunet, A. (2008). The FoxO code. *Oncogene, 27*(16), 2276-2288.

Castro, B., Barolo, S., Bailey, A.M., & Posakony, J.W. (2005). Lateral inhibition in proneural clusters: cis-regulatory logic and default repression by Suppressor of Hairless. *Development, 132*(15), 3333-3344.

Carlson, H., Ota, S., Song, Y., Chen, Y., & Hurlin, P.J. (2002). Tbx3 impinges on the p53 pathway to suppress apoptosis, facilitate cell transformation and block myogenic differentiation. *Oncogene, 21*(24), 3827-3835.

Chen, H.W., Marinissen, M.J., Oh, S.W., Chen, X., Melnick, M., Perrimon, N., Gutkind, J.S., & Hou, S.X. (2002). CKA, a novel multidomain protein, regulates the JUN N-terminal kinase signal transduction pathway in *Drosophila*. *Molecular and Cellular Biology, 22*(6), 1792-1803.

Clancy, D.J., Gems, D., Harshman, L.G., Oldman, S., Stocker, H., Hafen, E., Leevers, S.J., & Partridge, L. (2001). Extension of life-span by loss of CHICO, a *Drosophila* insulin receptor substrate protein. *Science, 292*(5514), 104-106.

Conlon, F.L., & Smith, J.C. (1999). Interference with brachyury function inhibits convergent extension, causes apoptosis, and reveals separate requirements in the FGF and activin signaling pathways. *Developmental Biology, 213*(1), 85-100.

Cubas, P., de Celis, J.F., Campuzano, S., & Modolell, J. (1991). Proneural clusters of *achaete-scute* expression and the generation of sensory organs in the *Drosophila* wing imaginal disc. *Genes & Development, 5*(6), 996-1008.

Curtis, J., & Mlodzik, M. (2000). Morphogenetic furrow initiation and progression during eye development in Drosophila: the roles of decapentaplegic, hedgehog and eyes absent. *Development, 127*(6), 1325-1336.

Das, S., Kumar, D., Zong, Y., Drescher, B., Morgan, S., & Leal, S. (2012). The T-box transcription factor *midline* collaborates with the insulin-regulated *dFOXO* transcription factor to regulate cell-fate specification in the developing eye of *Drosophila melanogaster*. Poster session presented at: Drosophila Genetics. 53rd Annual Conference of the Genetics Society of America, 2012 Mar 7-11. Chicago, IL.

Das, S., Chen, Q.B., Saucier, J.D., Drescher, B., Zong, Y., Morgan, S., Forstall, J., Meriwether, A., Toranzo, R., & Leal, S.M. (2013). The *Drosophila* T-box transcription factor Midline functions within the Notch-Delta signaling pathway to specify sensory organ precursor cell fates and regulates cell survival within the eye imaginal disc. *Mechanisms of Development, 130*(11-12), 577-601.

Degnan, B.M., Vervoort, M., Larroux, C., & Richards G.S. (2009). Early evolution of metazoan transcription factors. *Current Opinion in Genetics & Development, 19*(6), 591-599.

Doe, C.Q., Kuwada, J.Y., & Goodman, C.S. (1985). From epithelium to neuroblasts to neurons: the role of cell interactions and cell lineage during insect neurogenesis. *Philosophical Transactions of the Royal Society B: Biological Sciences, 312*(1153), 67-81.

Dutriaux, A., Godart, A., Brachet, A., & Silber, J. (2013). The insulin receptor is required for the development of the *Drosophila* peripheral nervous system. *PLoS ONE, 8*(9), e71857. doi:10.1371/journal.pone.0071857

Essers, M., Weijzen, S., de Vries-Smits, A.M., Saarloos, I., de Ruiter, N.D., Bos, J.L., & Burgering, B.M. (2004). FOXO transcription factor activation by oxidative stress mediated by the small GTPase Ral and JNK. *The European Molecular Biology Organization Journal, 23*(24), 4802–4812.

Formaz-Preston, A., Ryu, J.R., Svendsen, P.C., & Brook, W.J. (2012). The Tbx20 homolog Midline represses wingless in conjunction with Groucho during the maintenance of segment polarity. *Developmental Biology, 369*(2), 319-329.

Garofalo, R.S. (2002). Genetic analysis of insulin signaling in Drosophila. *Trends in Endocrinology & Metabolism, 13*(4), 156-162.

Garofalo, R.S., Orena, S.J., Rafidi, K., Torchia, A.J., Stock, J.L., Hildebrandt, A.L., Coskran, T., Black, S.C., Brees, D.J., Wicks, J.R., McNeish, J.D., & Coleman, K.G. (2003). Severe diabetes, age-dependent loss of adipose tissue, and mild growth deficiency in mice lacking Akt2/PKBβ. *Journal of Clinical Investigation, 112*(2), 197–208.

Geminard, C., Rulifson, E.J., & Leopold, P. (2009). Remote control of insulin secretion by fat cells in *Drosophila*. *Cell Metabolism, 10*(3), 199-207.

Georgescu, M. M. (2011). PTEN tumor suppressor network in PI3K-Akt pathway control. *Genes and Cancer, 1*(12), 1170-1177.

Greenwood, S., & Struhl, G. (1999). Progression of the morphogenetic furrow in the Drosophila eye: the roles of Hedgehog, Decapentaplegic and the Raf pathway. *Development, 126*(24), 5795-5808.

Greer, E.L., & Brunet, A. (2005). FOXO transcription factors at the interface between longevity and tumor suppression. *Oncogene, 24*(50), 7410-7425.

Grewal, S.S. (2009). Insulin/TOR signaling in growth and homeostasis: A view from the fly world. *The International Journal of Biochemistry & Cell Biology, 41*(5), 1006–1010.

Griffin, K.J., Stoller, J., Gibson, M., Chen, S., Yelong, D., Stainier, D.Y., & Kimelman, D. (2000). A conserved role for H15-related T-box transcription factors in zebrafish and Drosophila heart formation. *Developmental Biology, 218*(2), 235-247.

Glise, B., Bourbon, H., &Noselli, S. (1995). *Hemipterous* encodes a novel *Drosophila* MAP kinase kinase, required for epithelial cell sheet movement. *Cell, 83*(3), 451-461.

Glise, B., & Noselli, S. (1997). Coupling of Jun amino-terminal kinase and Decapentaplegic signaling pathways in *Drosophila* morphogenesis. *Genes & Development, 11*(13), 1738-1747.

Han, J., Richter, B., Li, Z., Kravchenko, V., & Ulevitch, R.J. (1995). Molecular cloning of human p38 MAP kinase. *Biochimica et Biophysica Acta, 1265*(2-3), 224-227.

Hartenstein, V., & Campos-Ortega, J.A. (1984). Early neurogenesis in wild-type *Drosophila melanogaster*. *Roux's Archives of Developmental Biology, 193*(5), 308-325.

Hay, B.A., Wolff, T., & Rubin, G.M. (1994). Expression of Baculovirus P35 prevents cell death in *Drosophila*. *Development, 120*(8), 2121-2129.

Hay, N. (2011). Interplay between FOXO, TOR, and Akt. *Biochimica et Biophysica Acta, 1813*(11), 1965-1970.

Heberlein, U., Wolff, T., & Rubin, G. M. (1993). The TGF beta homolog dpp and the segment polarity gene hedgehog are required for propagation of a morphogenetic wave in the Drosophila retina. *Cell, 75*(5), 913-926.

Helms, W., Lee, H., Ammerman, M., Parks, A.L., Muskavitch, M.A., & Yedvobnick, B. (1999). Engineered truncations in the *Drosophila* mastermind protein disrupt Notch pathway function. *Developmental Biology, 215*(2), 358-374.

Huang, H., Potter, C.J., Tao, W., Li, D.M., Brogiolo, W., Hafen, E., Sun, H., & Xu, T. (1999). PTEN affects cells size, cell proliferation and apoptosis during *Drosophila* eye development. *Development, 126*(23), 5365-5372.

Hsu, H.W., & Drummond-Barbosa, D. (2011). Insulin signals control the competence of the Drosophila female germline stem cell niche to respond to Notch ligands. *Developmental Biology, 350*(2), 290-300.

Ikeya, T., Galic, M., Belawat, P., Nairz, K., & Hafen, E. (2002). Nutrient-dependent expression of insulin-like peptides from neuroendocrine cells in the CNS contributes to growth regulation in *Drosophila*. *Current Biology, 12*(15), 1293-1300.

Jimenez, G., & Ish-Horowicz, D. (1997). A chimeric enhancer-of-split transcriptional activator drives neural development and achaete-scute expression. *Molecular and Cellular Biology, 17*(8), 4355-4362.

Junger, M.A., Rintelen, F., Stocker, H., Wasserman, J.D., Vegh, M., Radimerski, T., Greenberg, M.E., & Hafen, E. (2003). The *Drosophila* forkhead transcription factor FOXO mediates the reduction in cell number associated with reduced insulin signaling. *Journal of Biology, 2*(3), 20.

Kaltenbrun, E., Greco, T.M., Slagle, C.E., Kennedy, L.M., Tuo, L., Cristea, I.M., & Conlon, F.L. (2013). A Gro/TLE-NuRD corepressor complex facilitates Tbx20-dependent transcriptional repression. *Journal of Proteome Research, 12*(12), 5395-5409.

Kannan, K., & Fridell, Y-W.C. (2013). Functional implications of *Drosophila* insulin-like peptides in metabolism, aging, and dietary restriction. *Frontiers in Physiology, 4*, 288. Doi:10.3389/fphys.2013.00288

Kitamura, T., Kitamura, Y.I., Funahashi, Y., Shawber, C.J., Castrillon, D.H., Kollipara, R., DePinho, R.A., Kitajewski, J., & Accili, D. (2007). A Foxo/Notch pathway controls myogenic differentiation and fiber type specification. *Journal of Clinical Investigation, 117*(9), 2477-2485.

Kockel, L., Homsy, J.G. & Bohmann, D. (2001). *Drosophila* AP-1: lessons from an invertebrate. *Oncogene, 20*(19), 2347-2364.

Kraus, F., Haenig, B., & Kispert, A. (2001). Cloning and expression analysis of the mouse T-box gene Tbx20. *Mechanisms of Development, 100*(1), 87-91.

Kulisz, A., & Simon, H. G. (2008). An evolutionarily conserved nuclear export signal facilitates cytoplasmic localization of the Tbx5 transcription factor. *Molecular and Cellular Biology, 28*(5), 1553-1564.

Kuo, Y.C., Huang, K.Y., Yang, C.H., Yang, Y.S., Lee, W.Y., & Chiang, C.W. (2008). Regulation of Phosphorylation of Thr-308 of Akt, Cell Proliferation, and Survival by the B55α Regulatory Subunit Targeting of the Protein Phosphatase 2A Holoenzyme to Akt. *Journal of Biological Chemistry, 283*(4), 1882-1892.

Leal, S.M., Qian, L., Lacin, H., Bodmer, R., & Skeath, J.B. (2009). Neuromancer1 and Neuromancer2 Regulate Cell Fate Specification in the Developing Embryonic CNS of Drosophila melanogaster. *Developmental Biology, 325*(1), 138-150.

Lee, Y.S., & Carthew, R.W. (2003). Making a better vector for *Drosophila*: Use of intron spacers. *Methods, 30*(4), 322-329.

Leevers, S.J., Weinkove, D., MacDougall, L.K., Hafen, E., & Waterfield, M.D, (1996). The *Drosophila* phosphoinositide 3-kinase Dp110 promotes cell growth. *The European Molecular Biology Organization Journal, 15*(2), 6584-6594.

Li, W.Z., Li, S.L., Zheng, H.Y., Zhang, S.P., & Xue, L. (2012). A broad expression pattern profile of the GMR-Gal4 driver in *Drosophila melanogaster. Genetics and Molecular Research, 11*(3), 1997-2002.

Ligoxygakis, P., Yu, S.Y., Delidakis, C., & Baker, N.E. (1998). A subset of notch functions during *Drosophila* eye development requires *Su(H)* and the *E(spl)* gene complex. *Development, 125*(15), 2893-2900.

Lu, D., Huang, J., & Basu, A. (2006). Protein Kinase C activates Protein Kinase B/Akt via DNA-PK to Protect against Tumor Necrosis Factor-alpha-induced Cell Death. *Journal of Biological Chemistry, 281*(32), 22799-22807.

Luo, X., Puig, O., Hyun, J., Bohmann, D., & Jasper, H. (2007). Foxo and Fos regulate the decision between cell death and survival in response to UV irradiation. *The European Molecular Biology Organization Journal, 26*(2), 380-390.

Maehama, T., Kosaka, N., Okahara, F., Takeuchi, K., Umeda, M., Dixon, J.E., & Kanaho, Y. (2004). Suppression of a phosphatidylinositol 3-kinase signal by a specific spliced variant of *Drosophila* PTEN. *FEBS Letters, 565*(1-3), 43-47.

Mattila, J., Kallojarvi, J., & Puig, O. (2008). RNAi screening for kinases and phosphatases identifies FoxO regulators. *Proceedings of the National Academy of Sciences, 105*(39), 14873-14878.

McCubrey, J.A., LaHair, M.M., & Franklin, R.A. (2006). Reactive Oxygen Species-Induced Activation of the MAP Kinase Signaling Pathways. *Antioxidants & Redox Signaling, 8*(9-10), 1775-1789.

Meins, M., Henderson, D.J., Bhattacharya, S.S., & Sowden, J.C. (2000). Characterization of the human TBX20 gene, a new member of the T-box gene family closely related to the *Drosophila* H15 gene. *Genomics, 67*(3), 317-332.

Miskolczi-McCallum, C.M., Scavetta, R.J., Svendsen, P.C., Soanes, K.H., & Brook, W.J. (2005). The *Drosophila melanogaster* genes *midline* and *H15* are conserved regulators of heart development. *Developmental Biology, 278*(2), 459-472.

Mollace, V., Iannone, M., Muscoli, C., Palma, E., Granato, T., Rispoli, V., Nistico, R., Rotiroti, D., & Salvemini, D. (2003). The role of oxidative stress in paraquat-induced neurotoxicity in rats: protection by non peptidyl superoxide dismutase mimetic. *Neuroscience Letters, 335*(3), 163-166.

Muller, C.W., & Herrmann, B.G. (1997). Crystallographic structure of the T domain-DNA complex of the Brachyury transcription factor. *Nature, 389*(6653), 884-888.

Muskavitch, M.A. (1994). Delta-notch signaling and *Drosophila* cell fate choice. *Developmental Biology, 166*(2), 415-430.

Nagel, A.C., Krejci, A., Tenin, G., Bravo-Patino, A., Bray, S., Maier, D., & Preiss, A. (2005). Hairless-mediated repression of Notch target genes requires the combined activity of Groucho and CtBP corepressors. *Molecular and Cellular Biology, 25*(23), 10433-10441.

Nagel, A.C., & Preiss, A. (2011). Fine tuning of Notch signaling by differential co-repressor recruitment during eye development of *Drosophila*. *Hereditas, 148*(3), 77-84.

Nam, Y., Piotr, S., Pear, W.S., Aster, J.C., & Blacklow, S.T. (2007). Cooperative assembly of high-order Notch complexes functions as a switch to induce transcription. *Proceedings of the National Academy of Sciences, 104*(7), 2103-2108.

Ni, J.Q., Liu, L.P., Binari, R., Hardy, R., Shim, H.S., Cavallaro, A., Booker, M., Pfeiffer, B.D., Markstein, M., Wang, H., Villalta, C., Laverty, T.R., Perkins, L.A., & Perrimon, N. (2009). A *Drosophila* resource of transgenic RNAi lines for neurogenetics. *Genetics, 182*(4), 1089-1100.

Nielsen, M.D., Luo, X., Biteau, B., Syverson, K., & Jasper, H. (2008). 14-3-3ε antagonizes FoxO to control growth, apoptosis and longevity in Drosophila. *Aging Cell, 7*(5), 688–699.

Oldham, S., Stocker, H., Laffargue, M., Wittwer, F., Wymann, M., & Hafen, E. (2002). The *Drosophila* insulin/IGF receptor controls growth and size by modulating PtdInsP(3) levels. *Development, 129*(17), 4103-4109.

Penton, A., Selleck, S.B., & Hoffman, F.M. (1997). Regulation of cell cycle synchronization by decapentaplegic during *Drosophilia* eye development. *Science, 275*(5297), 203-206.

Perry, M.M. (1968). Further studies on the development of *Drosophila melanogaster*. II. The interommatidial bristles. *Journal of Morphology*, *124*(2), 249-262.

Poeck, B., Hofbauer, A., & Pflugfelder, G.O. (1993). Expression of the *Drosophilia optomotor-blind* gene transcript in neuronal and glial cells of the developing nervous system. *Development, 117*(3), 1017-1029.

Porsch, M., Hofmeyer, K., Bausenwein, B.S., Grimm, S., Weber, B.H.F., & Miassod, R., (1998). Isolation of a Drosophila T-box gene closely related to human TBX1. *Gene, 212*(2), 237–248.

Puig, O., Marr, M.T., Ruhf, L., & Tjian, R. (2003). Control of cell number by *Drosophila* FOXO: downstream and feedback regulation of the insulin receptor pathway. *Genes & Development, 17*, 2006-2020.

Puig, O., & Tjian, R. (2005). Transcriptional feedback control of the insulin receptor by dFOXO/FOXO1. *Genes & Development, 19*(20), 2435-2446.

Qian, L., Liu, J., & Bodmer, R. (2005). Neuromancer TBX20-related genes (*H15/midline*) promote cell fate specification and morphogenesis of the *Drosophila* heart. *Developmental Biology*, *279*(2), 509-524.

Ready, D.F., Hanson, T.E., & Benzer, S. (1976). Development of the Drosophila retina, a neurocrystalline lattice. *Developmental Biology*, *53*(2), 217-240.

Rebeiz, M., Miller, S.W., & Posakony, J.W. (2011). Notch regulates *numb*: integration of conditional and autonomous cell fate specification. *Development, 138*(2), 215-225.

Reim, I., Lee, H.H., & Frasch, M. (2003). The T-box-encoding Dorsocross genes function in amnioserosa development and the patterning of the dorsolateral germ band downstream of Dpp. *Development, 130*(14), 3187-3204.

Reim, I., Mohler, J.P., & Frasch M. (2005). Tbx20-related genes, *mid* and *H15*, are required for *tinman* expression, proper patterning, and normal differentiation of cardioblasts in *Drosophila*. *Mechanisms of Development, 122*(9), 1056-69.

Renault, T.T., Teijido, O., Antonsson, B., Dejean, L.M., & Manon, S. (2013). Regulation of Bax mitochondrial localization by Bcl-2 and Bcl-xl: Keep your friends close but your enemies closer. *International Journal of Biochemistry and Cell Biology, 45*(1), 64-67.

Riesgo-Escovar, J.R., Jenni, M., Fritz, A., & Hafen, E. (1996). The *Drosophila* Jun-N-terminal kinase is required for cell morphogenesis but not for DJun-dependent cell fate specification in the eye. *Genes & Development, 10*(21), 2759-2768.

Rockwell, C.E., Zhang, M., Fields, P.E., & Klaassen, C.D. (2012). Th2 skewing by activation of Nrf2 in CD4(+) T cells. *Journal of Immunology, 188*(4), 1630-1637.

Ruaud, A.F., & Thummel, C.S. (2008). Serotonin and insulin signaling team up to control growth in Drosophila. *Genes & Development, 22*(14), 1851-1855.

Rulifson E.J., Kim, S.K., & Nusse, R. (2002). Ablation of insulin-producing neurons in flies: growth and diabetic phenotypes. *Science, 296*(5570), 1118-1120.

Ryoo, H.D., Gorenc, T., & Steller, H. (2004). Apoptotic cells can induce compensatory cell proliferation through the JNK and the Wingless signaling pathways. *Developmental Cell, 7*(4), 491-501.

Rhyu et al., Jan, L.Y., & Jan, Y.N. (1994). Asymmetric distribution of numb protein during division of the sensory organ precursor cell confers distinct fates to daughter cells. *Cell, 76*(3), 477-491.

Sakabe, N.J., Aneas, I., Shen T., Shokri, L., Park S.Y., Bulyk, M.L., Evans, S.M., & Nobrega, M.A. (2012). Dual transcriptional activator and repressor roles of TBX20 regulate adult cardiac structure and function. *Human Molecular Genetics, 21*(10), 2194-2204.

Schroeter, E.H., Kisslinger, J.A., & Kopan, R. (1998). Notch-1 signaling requires ligand-induced proteolytic release of intracellular domain. *Nature, 393*(6683), 382-386.

Shen, T., Yang, C., Ding, L., Zhu, Y., Ruan, Y., Cheng, H., Qin, W., Huang, X., Zhang, H., Man, Y., Liu, D., Wang, S., Bian, Y., Xiao, C., Zhao, Y., & Li, J. (2013). Tbx20 functions as an important regulator of estrogen-mediated cardiomyocyte protection during oxidative stress. *International Journal of Cardiology, 168*(4), 3704-3714.

Skeath, J.B., & Caroll, S.B. (1991). Regulation of *achaete-scute* gene expression and sensory organ pattern formation in the *Drosophila* wing. *Genes & Development, 5*(6), 984-995.

Skeath, J.B., & Caroll, S.B. (1994). The *achaete-scute* complex: generation of cellular pattern and fate within the *Drosophila* nervous system. *The Journal of the Federation of American Societies for Experimental Biology, 8*(10), 714-721.

Skeath, J.B., & Doe, C.Q. (1996). The *achaete-scute* complex proneural genes contribute to neural precursor specification in the *Drosophila* CNS. *Current Biology, 6*(9), 1146-1152.

Sluss, H.K., Han, Z., Barrett, T., Goberdhan, D.C., Wilson, C., Davis, R.J., & Ip, Y.T. (1996). A JNK signal transduction pathway that mediates morphogenesis and an immune response in *Drosophila*. *Genes & Development, 10*(21), 2745-2758.

Stennard, F.A., Costa, M.W., Elliott, D.A., Rankin, S., Haast, S.J., Lai, D., McDonald, L.P., Niederreither, K., Dolle, P., Bruneau, B.G., Zorn, A.M., & Harvey, R.P. (2003). Cardiac T-box factor Tbx20 directly interacts with Nkx2-5, GATA4, and GATA5 in regulation of gene expression in the developing heart. *Developmental Biology, 262*(2), 206-224.

Sunayama, J., Tsuruta, F., Mayuyama, N., & Gotoh, Y. (2005). JNK antagonizes Akt-mediated signals by phosphorylating 14-3-3. *Journal of Cell Biology, 170*(2), 295-304.

Svendsen, P.C., Formaz-Preston, A., Leal, S.M., & Brook, W.J. (2009). The Tbx20 homologs midline and H15 specify ventral fate in the Drosophila melanogaster leg. *Development, 136*(16), 2689-2693.

Szabo, S.J., Kim, S.T., Costa, G.L., Zhang, X., Fathman, C.G., & Glimcher, L.H. (2000). A novel transcription factor, T-bet, directs Th1 lineage commitment. *Cell, 100*(6), 655-669.

Tettweiler, G., Miron, M., Jenkins, M., Sonenberg, N., & Lasko, P.F. (2005). Starvation and oxidative stress resistance in *Drosophila* are mediated through the sIF4E-binding protein, d4E-BP. *Genes & Development, 19*(16), 1840-1843.

Tomlinson, A., & Ready, D.F. (1987). Cell fate in the Drosophila ommatidium. *Developmental Biology, 123*(1), 264-275.

Treisman, J.E., & Rubin, G.M. (1995). *wingless* inhibits morphogenetic furrow movement in the *Drosophila* eye disc. *Development, 121*(11), 3519-3527.

Tsuruta, F., Sunayama, J., Mori, Y., Hattori, S., Shimizu, S., Tsujimoto, Y., Yoshioka, K., Masuyama, N., & Gotoh, Y. (2004). JNK promotes Bax translocation to mitochondria through phosphorylation of 14-3-3 proteins. *The European Molecular Biology Organization Journal, 23*(8), 1889-1899.

Tu, M.P., & Tatar, M. (2003). Juvenile diet restriction and the aging and reproduction of adult Drosophila melanogaster. *Aging Cell, 2*(6), 327-333.

Tzivion, G., Dobson, M., & Ramakrishnan, G. (2011). FoxO transcription factors; regulation by AKT and 14-3-3 proteins. *Biochimica et Biophysica Acta, 1813*(11), 1938-1945.

Udvardy, A., & Schedl, P. (1984). Chromatin organization of the 87A7 heat shock locus of *Drosophila melanogaster*. *Journal of Molecular Biology, 172*(4), 385-403.

Vanhaesebroeck, B., & Aless, D.R, (2000). The PI3K–PDK1 connection: more than just a road to PKB. *Biochemical Journal, 346*(Pt 3), 561–576.

Vanhaesebroeck, B., & Waterfield, M.D. (1999). Signaling by Distinct Classes of Phosphoinositide 3-Kinases. *Experimental Cell Research, 253*(1), 239–254.

Vecchione, A., Marchese, A., Henry, P., Rotin, D., & Morrione, A. (2003). The Grb10/Nedd4 Complex Regulates Ligand-Induced Ubiquitination and Stability of the Insulin-Like Growth Factor I Receptor. *Molecular and Cellular Biology, 23*(9), 3363-3372.

Waddington, C.H., & Perry, M.M. (1960). The ultrastructure of the developing eye of *Drosophila*. *Proceedings of the Royal Society B: Biological Sciences, 153*(951), 155-178.

Wang, M.C., Bohmann, D., & Jasper, H. (2005). JNK extends life span and limits growth by antagonizing cellular and organism-wide responses to insulin signaling. *Cell, 121*(1), 115-125.

Weston, C.R., & Davis, R.J. (2007). The JNK signal transduction pathway. *Current Opinion in Cell Biology, 19*(2), 142-149.

Wiersdorff, V., Lecuit, T., Cohen, S.M., & Mlodzik, M. (1996). Mad acts downstream of Dpp receptors, revealing a differential requirement for dpp signaling in initiation and propagation of morphogenesis in the Drosophila eye. *Development, 122*(7), 2153-62.

Zecchini, V., Brennan, K., & Martinez-Arias, A. (1999). An Activity of Notch regulates JNK signalling and affects dorsal closure in Drosophila. *Current Biology, 9*(9), 460-469.

Zhang, H., Stallock, J.P., Ng, J.C., Reinhard, C., & Neufeld, T.P. (2000). Regulation of cellular growth by the *Drosophila* target of rapamycin dTOR. *Genes & Development, 14*(21), 2712-2724.